FACULDADE DE ENGENHARIA DA UNIVERSIDADE DO PORTO

FEUP

Modulation Analysis for an Underwater Communication Channel

Júlio Diogo Miranda Xavier

Mestrado Integrado em Engenharia Electrotécnica e de Computadores

Supervisor: Artur Manuel Oliveira Andrade de Moura (PhD)

31 October 2012

Resumo

Nos últimos anos, a comunidade científica tem dedicado recursos consideráveis para a pesquisa de comunicações sem fio subaquáticas, com especial ênfase na comunicação acústica.

Esta tese resulta de uma parceria com uma equipa da *Universidade do Minho* que tem vindo a trabalhar num projeto de comunicação acústica subaquática. O trabalho aqui apresentado está focado na definição de um modelo de canal, melhorando o modelo já desenvolvido e adicionando o efeito multipercurso. Espera-se que, com este modelo, os resultados da simulação sejam mais próximos do que é observado ou esperado num ambiente real.

Além disso, várias modulações digitais foram estudadas e algumas foram consideradas nas simulações realizadas para avaliar os seus desempenhos relativos. Um foco especial foi dado sobre o efeito multipercurso e concluiu-se que este fenómeno pode ser um sério entrave nestas comunicações. Em situações em que a sua presença seja relevante, devem ser ponderadas o uso de modulações de comunicação mais complexas, como Orthogonal Frequency Division Multiplexing (OFDM), que é capaz de remover ou de reduzir significativamente o efeito aditivo ou subtrativo do multipercurso, de modo a obter um sinal adequado na extremidade receptora.

Abstract

In recent years the scientific community has devoted considerable resources to the research of wireless underwater communications, with a particular emphasis on acoustic communications.

This thesis is the result of a partnership with a team at the *Universidade do Minho* that has been working in an acoustic underwater communications project. The work presented herein is centered on the channel model definition, improving the model already developed and adding the multipath effect. It is expected that, with this model, simulation results will be closer to what is observed or expected in a real environment.

Additionally, various digital modulations were studied and some were considered in the simulations performed to evaluate their relative performances. A particular focus was placed on the multipath effect and it was concluded that this phenomenon can be a serious impediment to underwater communications. In fact, when present, it must be taken into account and more complex communication modulations schemes, like Orthogonal Division Frequency Multiplexing (OFDM), which is able to remove or significantly reduce the multipath impairment, must be considered in order to obtain an adequate signal at the receiver end.

Aknowlegdements

My academic studies have constituted a long journey, during which were always present the comfort, understanding and friendship, provided by my family, friends, colleagues and teachers. To all of them, a heartfelt Thank You.

I would also like to thank the great support, comprehension and effort given to me by my supervisor Professor Artur Moura (PhD), Professor Joaquim Costa (PhD), the PhD student Marcos Martins from *Universidade do Minho* and the team from the Universidade do Minho. Their contribution to this Master Degree dissertation project has been fundamental.

Júlio Xavier

"Necessity keeps the mind sharp"

Popular Proverb

Contents

1 Introduction **1**
- 1.1 Motivation and Objectives . . . 1
- 1.2 Dissertation structure . . . 2

2 State-of-the-art on UWAC **3**
- 2.1 Introduction . . . 3
- 2.2 Some UWAC History . . . 3
- 2.3 UWAC Fundamentals . . . 4
  - 2.3.1 Sound . . . 4
  - 2.3.2 Acoustic waves . . . 5
  - 2.3.3 Acoustic source level . . . 7
- 2.4 Underwater Channel characteristics . . . 8
  - 2.4.1 Spreading loss . . . 9
  - 2.4.2 Absorption loss . . . 9
  - 2.4.3 Path loss . . . 11
  - 2.4.4 Channel bandwidth . . . 11
  - 2.4.5 Noise . . . 12
  - 2.4.6 Propagation delay . . . 12
  - 2.4.7 Multipath . . . 13
  - 2.4.8 Doppler effect . . . 14
- 2.5 Research on UWAC . . . 14

3 Modulation Techniques **15**
- 3.1 Analog and digital modulations . . . 15
  - 3.1.1 Types of modulation . . . 15
- 3.2 Analog modulations . . . 16
- 3.3 Digital modulations . . . 16
  - 3.3.1 Binary modulations . . . 17
  - 3.3.2 *M*-ary modulations . . . 20
  - 3.3.3 Bandwidth Efficiency . . . 24
  - 3.3.4 Orthogonal Frequency Division Multiplexing . . . 25

4 UWAC Project **27**
- 4.1 UWAC set-up at *Universidade do Minho* . . . 27
  - 4.1.1 Projectors and Hydrophones . . . 27
  - 4.1.2 Amplifiers . . . 28
  - 4.1.3 Signal generator . . . 28

4.1.4 Picoscope . . . 29
4.1.5 FPGAs . . . 29
4.2 System model . . . 30
4.3 Aquatic chanel model . . . 30
4.3.1 Attenuation block . . . 31
4.3.2 Noise block . . . 32
4.3.3 Doppler effect block . . . 32
4.3.4 Propagation delay block . . . 32
4.4 The multipath block . . . 32
4.4.1 Multipath Channel Transfer Function . . . 32
4.4.2 Equations for multipath calculation . . . 33
4.5 Software tool used for the simulations . . . 34
4.6 Extra Tasks . . . 35
4.6.1 OFDM experiments . . . 35
4.6.2 Graphical User Interface application . . . 35

5 Simulations and results **37**
5.1 Path loss . . . 37
5.2 Binary digital modulations simulated and results . . . 37
5.2.1 OOK modulation . . . 39
5.2.2 BASK modulation . . . 40
5.2.3 BPSK modulation . . . 40
5.2.4 BFSK modulation . . . 42
5.3 Chapter conclusions . . . 44

6 Conclusions and Future Work **47**
6.1 Results achieved . . . 47
6.2 Future developments . . . 48

A Schematics and schemes **49**
A.1 Schematic of the complete underwater system . . . 49
A.2 Schematic of the aquatic channel . . . 50
A.3 Aquarium multipath schemes . . . 50

B MatLab blocks and modules code **55**
B.1 Attenuation code . . . 55
B.2 Multipath code . . . 59
B.3 Filter code . . . 61
B.4 Ambient noise code . . . 62
B.5 Signal with added noise code . . . 63
B.6 Attenuation profiles . . . 64
B.7 Attenuation function . . . 67

C Channel GUI application for MatLab with multipath calculator tool **71**
C.1 GUI figure 1 . . . 71
C.2 GUI example 2 . . . 72
C.3 GUI example 3 . . . 73
C.4 GUI example 4 . . . 74

D Multipath MatLab application **75**
D.1 MatLab example of multipath with Rayleigh channel model 75
D.2 MatLab figure application of multipath with Rayleigh channel model with diverse analysis . 76

References **79**

List of Figures

2.1 The experiment to measure the sound in water . . . 4
2.2 Temperature, salinity and pressure dependence with depth . . . 6
2.3 Sound speed vs. depth . . . 6
2.4 Examples of different patterns for acoustic radiating sources: a) aperture angle is 0^o; b) aperture angle is 30^o; c) aperture angle is 60^o. . . . 7
2.5 Absorption coefficients . . . 11
2.6 Multipath in a transmission . . . 13
2.7 Doppler shift . . . 14

3.1 Conventional AM modulation . . . 16
3.2 Conventional PM and FM modulations . . . 17
3.3 Waveforms for the simplest binary digital modulations . . . 17
3.4 BPSK constellation and BER expression . . . 18
3.5 Binary CPFSK waveform . . . 19
3.6 BFSK constellation and BER expression . . . 19
3.7 BER performance of binary digital modulations . . . 20
3.8 Interpretation of the eye pattern . . . 21
3.9 8PSK constellation and symbol error probability expression . . . 22
3.10 QPSK constellation and BER relation with BPSK case . . . 22
3.11 16QAM constellation and BER expression . . . 23
3.12 BER performance of M-ary digital modulations . . . 23
3.13 BER Performance of MFSK modulation . . . 24
3.14 OFDM basic principle for avoiding multipath effects . . . 25
3.15 OFDM system block diagram . . . 25

4.1 Projector and hydrophone . . . 28
4.2 Transmitter Receiver amplifiers . . . 28
4.3 Signal generator . . . 29
4.4 Picoscope . . . 29
4.5 FPGA device used at *Universidade do Minho* for the UWAC project . . . 30
4.6 System block diagram and the aquatic block model . . . 31
4.7 Aquatic block model . . . 31
4.8 Aquarious for test purposes . . . 33
4.9 Rayleygh multipath UWAC model with BPSK . . . 35
4.10 2D Source plot beam pattern . . . 36
4.11 Multipath in MatLab GUI application . . . 36

5.1 Attenuation, spreading and absorption . . . 38

5.2 Dependence of absorption components with frequency . . . 39
5.3 Individual plots of the four components of absorption . . . 40
5.4 OOK signal at the channel input . . . 41
5.5 OOK signal at the channel output . . . 41
5.6 BASK signal at the channel input . . . 42
5.7 BASK signal at the channel input . . . 42
5.8 BPSK signal at the channel inpu . . . 43
5.9 BPSK signal at the channel inpu . . . 43
5.10 BFSK signal at the channel input . . . 44
5.11 BFSK signal at the channel output . . . 44

A.1 Underwater communication system model . . . 49
A.2 Module of aquatic channel . . . 50
A.3 First case of reflection . . . 51
A.4 Second case of reflection . . . 52
A.5 Third case of reflection . . . 53

C.1 GUI application: example window 1 . . . 71
C.2 GUI application: example window 2 . . . 72
C.3 Minimum multipath calculator tool . . . 73
C.4 GUI application: example window 3 . . . 74

D.1 Multipath channel Graphical User Interface application in MatLab . . . 76
D.2 Simulink model for testing BPSK with a multipath Rayleigh channel . . . 77
D.3 Simulink model for testing OFDM with a multipath Rayleigh channel . . . 77

List of Tables

2.1 Typical values of the sound velocity in fluids (25°C) 7
2.2 Bandwidth available at different ranges 12

3.1 Bandwidth B and efficiency ε for various modulation types 24

5.1 Other parameters used in simulations 38

Abbreviations

ADC	Analog to Digital Converter
AM	Amplitude Modulation
AUV	Autonomous Underwater Vehicles
AWGN	Additive White Gaussian Noise
BER	Bit Error Rate
BPF	Band Pass Filter
BPSK	Binary Phase Shift Keying
BW	Bandwidth
DAC	Digital to Analog Converter
erfc	Complementary Error Function
FDM	Frequency Division Multiplexing
FM	Frequency Modulation
ISI	Inter Symbol Interference
LOS	Line-Of-Sight link
LPF	Low Pass Filter
MPSK	Multiple Phase Shift Keying
OFDM	Orthogonal Frequency Division Multiplexing
PDF	Probability Density Function
PRBS	Pseudo-Random Binary Sequence
PSD	Power Spectrum Density
PSK	Phase-Shift Keying
PVDF	Polyvinylidene Fluoride
PZT	Lead Zirconate Titanate
QAM	Quadrature Amplitude Modulation
RL	Reflective Link
RRC	Root Raised Cosine
SEL	Sound Exposure Level
SNR	Signal-to-Noise Ratio
SONAR	SOund Navigation and Ranging
SP	Salinity Profile
SVP	Sound Velocity Profile
TDM	Time Division Multiplexing
TP	Temperature Profile
u.a.	Unit Arbitrary
USNs	Underwater Sensor Nodes
UUV	Unmanned Underwater Vehicle
UWAC	UnderWater Acoustic Communications
UUVs	Unmanned Underwater Vehicles

Symbols

A	Amplitude
agi	Angle of Incidence
B	Bandwidth
BER	Bit Error Rate
(CX,CY,CZ)	Canal Coordinates
c	Sound Speed
D	Depth
pH	Acidity of Water
rr	Reference Transducer Radius
r	Transducer Radius
dB	Decibel
I	Acoustic Intensity
ISI	InterSymbolic Interference
LPF	Low Pass Filter
Mev	Manually Entered Value
Ns	ShipNoise
Nt	TurbulenceNoise
Nth	ThermalNoise
Nw	WaveNoise
PDF	Probability Density Function
pss	Piezo Sound Speed
pd	Piezo Density
pt	Piezo Thickness
sps	Samples Per Second
P	Acoustic Pressure
PRBS	Pseudo-Random Binary Sequence
PSD	Power Spectrum Density
(RX,RY,RZ)	Receiver Coordinates
rms	Root Mean Square
RRC	Root Raised Cosine
S	Salinity
s	Shipping Factor
SNR	Signal-to-Noise Ratio
(TX,TY,TZ)	Transmitter Coordinates
T	Temperature
w	Wind Speed
Z	Acoustic Impedance

Chapter 1

Introduction

This document constitutes the master thesis report for the *MIEEC* course at the *Faculdade de Engenharia da Universidade do Porto* . It documents all the work done to complete the objectives which were beforehand prepared for a partnership project with a team from the *Universidade do Minho* , which has been developing work in the area of underwater communications.

1.1 Motivation and Objectives

Discovering and exploring new environments is an important human endeavor, a motor for mankind's evolution. One vast environment which is still much unexplored is the underwater world. Crucial for its successful exploration are reliable communication systems.

The topic is complex and there are various difficulties in underwater communications, such as water chemical constitution, environmental variables, and the presence of various types of noise.

A promising solution, which has been studied and implemented for communicating within this environment, is the use of acoustic waves for the transmission of signals. Electromagnetic waves usually are not considered as a solution for underwater communications because their attenuation is too high. Acoustic waves appear as a good alternative, despite some associated negative aspects. For long communicating distances, an abrupt decay in pressure may occur, impairing the communication quality. This phenomenon may occur even for medium distances and it is dependent of the transmitting acoustic wave frequency.

The introduction of intermediate sensor networks leads to increases in the data rate and to an improvement of the transmission quality, thus bettering the capacity of the overall communication system.

Our work is focused on the area of communication channels, particularly the multipath effect and its impact on the system performance, and it is based on the model developed at the *Universidade do Minho* by Diogo Mendes [1]. For this project, that model has been modified, so as to be able to study the system behavior under various modulation techniques. Our goal is to add a multipath interference effect to the underwater

acoustic channel model previously created [1], getting closer to more realistic scenarios. Various modulation techniques have been tested and analyzed, in order to understand their behavior in such communication channel and decide which ones are more suitable, depending on the actual channel characteristics.

The interest from the research community in the area of underwater communications has increased recently and this work aims to be a contribution to the development of the UnderWater Acoustic Communication (UWAC) field.

1.2 Dissertation structure

This document is organized as follows. Chapter 1 describes the motivation for the work and also some introductory insight to the theme of this project. Chapter 2 presents a literature review on UWAC, the approaches that are being used and all the techniques applied in this field. The communication using acoustic signals in general is also described in this chapter. Modulation techniques that are applied in communications in general are addressed in chapter 3. Chapter 4 contains a description of the system model, focussing in detail the channel, as well as some extra tasks. Simulation results run with MatLab, which constitute a relevant contribution of this work, are included in Chapter 5. Finally, Chapter 6 discusses relevant conclusions from this thesis and future developments of this work.

Chapter 2

State-of-the-art on UWAC

In this chapter a very brief summary of the Underwater Acoustic Communications (UWAC) history is presented. Then follows a description of the fundamentals and relevant physical quantities related to UWAC, as they will be important in understanding the work developed in this thesis. Finally, a very brief description of recent activities in this field is shown.

2.1 Introduction

The Earth planet is 70% [2] water covered and most of this extensive area is still largely unknown and unexplored. Research in UWAC is important in many aspects, namely for studying underwater ecosystems, for exploring underwater natural resources, for predicting possible natural disasters and also for defense purposes.

2.2 Some UWAC History

The area of UWAC has experienced significant research over the last decades, which led to recent progress in this endeavor. This interest started many years ago when Jean Daniel Colladon, a physicist/engineer, and Charles-Francois Sturn, a mathematician, performed an experiment, back in 1826, which can be thought as the starting point for underwater communications. The experiment took place in the Geneva Lake, in Switzerland, and they used a church bell to prove that sound travels faster in water than in air. One of them lighted a gunpowder flash and at the same time struck the church bell that was underwater. The other started the clock when he saw the gunpowder flash and only stopped it when he heard the noise made by the church bell (to do so he used a trumpet placed underwater as can be seen in figure 2.1). The distance that separated the two boats in this experiment was around 10 miles. Despite their simple instruments, they obtained a sound speed in water of 1435 m/s. This measurement was remarkably accurate, considering that the value obtained is not too far from currently known values, approximately 1500 m/s [3]. Going

further back in time, Leonardo da Vinci, a genius in several fields, imagined how one would be able to produce acoustic waves in water and then see what would happen at a distant place, when trying to listen to those waves. Nowadays, fortunately, we have ever-better means and knowledge basis to explore underwater acoustic communications and, not surprisingly, this field of research is now very active.

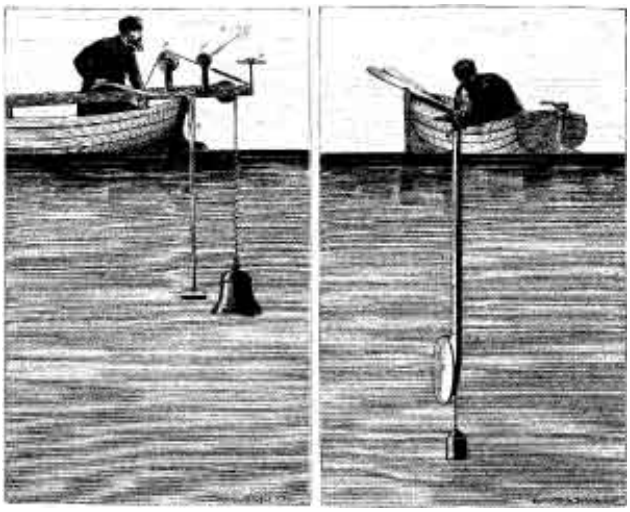

Figure 2.1: The experiment to measure the sound in water

2.3 UWAC Fundamentals

As in the electrical area, there are also in acoustics important physical quantities that must be described to give the necessary background associated with this field of knowledge.

2.3.1 Sound

Sound is produced when an object vibrates and transmits his motion to the surrounding physical medium. This results in propagation of vibrations where the particles in the medium oscillate in the same direction of the propagation, so we have what is called a longitudinal wave.

2.3.1.1 Acoustic pressure

Given a plane wave, acoustic Pressure (P), with unit Pa or N/m^2, is defined by the following equation

$$P = \rho_0 cv = \rho c 2\pi f \xi \quad \xi = \frac{v}{2\pi f} \tag{2.1}$$

where ρ_0 represents the fluid density, c is the velocity of the sound wave propagation and v is the particle velocity. The variable v is equivalent to $\xi 2\pi f$. This quantity P is analogous to the potential difference in electrical circuits.

The quantity $\rho_0 c$ is called specific impedance and has the same role has the intrinsic impedance defined for a transverse electromagnetic.

2.3.1.2 Acoustic impedance

The acoustic impedance is given by:

$$Z = \frac{P}{U} \tag{2.2}$$

where U is the acoustic volume flow. This equation is analogous to Ohm's law and Z is a function of frequency, with real and imaginary components.

2.3.1.3 Acoustic intensity

The acoustic intensity I (unit W/m^2) is the energy per second that crosses the unit area. For a plane wave it is given by:

$$I = Pv \tag{2.3}$$

so that it may be viewed as the acoustic power density produced by the source.

Normally, a reference intensity I_r is defined for each medium under certain circumstances. For example, the underwater reference intensity is the one produced by a plane wave with root mean square pressure of $1\mu Pa$.

2.3.2 Acoustic waves

As an example, the wave equation of a baffled piston projector, a circular kind of projector, in spherical coordinates (r, θ, ϕ),is given by:

$$\tilde{P}(r,\theta,t) = \underbrace{j\rho c \frac{Qk}{2\pi r} e^{(\omega t - kr)}}_{(1)} \underbrace{\frac{2J_1(ka\sin\theta)}{ka\sin\theta}}_{(2)} \tag{2.4}$$

where the first term (1) represents a spherical wave generated by what is called an ideal omnidirectional source. The second term (2), which depends of θ and the Bessell function of the first kind, represents the directivity of the actual source. It gives us an idea on how the source concentrates more energy on certain spacial directions. This is very analogous to the antenna field theory and we can, in a similar way, define the near field and the far field. This second one is of interest from the acoustic wave propagation point of view,

as it can be approximated by a one dimension frontwave and it can be treated as a ray, or a sum of rays, in different directions, when the distance is longer than the wavelength [4].

2.3.2.1 Sound speed profiles

Sound speed in water depends of several parameters, such as temperature, salinity and pressure. Figure 2.2 shows how these parameters change with depth, for the open ocean case. As a consequence, for open

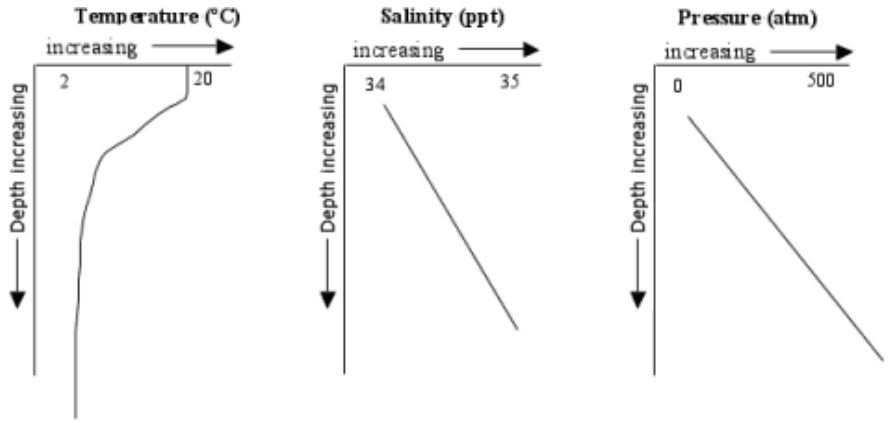

Figure 2.2: Temperature, salinity and pressure dependence with depth

ocean sound speed follows the profile depicted in figure 2.3 [5], [6], [7], [3].

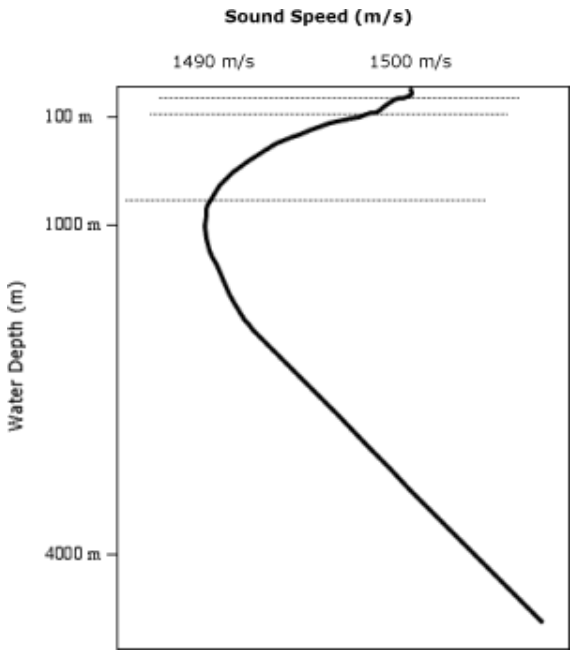

Figure 2.3: Sound speed vs. depth

For comparison purposes, table 2.1 shows the diversity of values for the speed of sound in some gases and in some liquids [8] .

Table 2.1: Typical values of the sound velocity in fluids (25°C)

Gas	Velocity (m/s)	Liquid	Velocity (m/s)
Air	331	Carbon tetrachloride (CCl_4)	929
Carbon dioxide (CO_2)	259	Ethanol (C_2H_6O)	1207
Hydrogen (H_2)	1284	Ethylene glycol ($C_2H_6O_2$)	1658
Methane (CH_4)	430	Glycerol ($C_3H_8O_3$)	1904
Oxygen (O_2)	316	Mercury (Hg)	1450
Helium (H_2)	213	Water (distilled)	1498
Oxygen (O_2)	1016	Water (sea)	1531

2.3.2.2 Wave propagation patterns

The radiation pattern of an acoustic source is a $3D$ representation of the signal intensity. The shape of the pattern can vary, depending of the type of source used and, thus, it can exhibit different aperture angles, as can be seen in figure 2.4. Notice also that only one lobe may be present or, when the source is more directive, there is a narrow lobe, called principal lobe, and sidelobes of lower maximum levels.

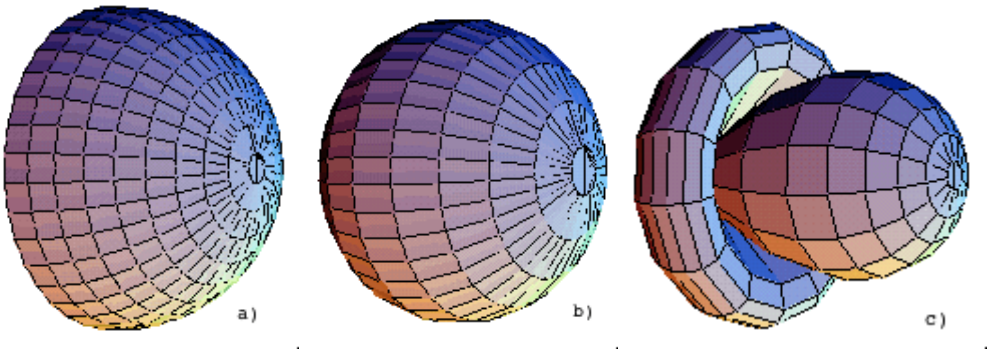

Figure 2.4: Examples of different patterns for acoustic radiating sources: a) aperture angle is 0°; b) aperture angle is 30°; c) aperture angle is 60°.

2.3.3 Acoustic source level

The source level quantity associated with a projector, $SL_{projector}$, is commonly defined in terms of the sound pressure level at a well-defined distance of 1m from its acoustic center. The source intensity at this reference point is:

$$I = \frac{P_{tx}}{Area} \quad (W/m^2) \tag{2.5}$$

and is measured in $dB're1\mu Pa'$, meaning: relative to the intensity due to a pressure of $1\mu Pa$. For an omni-directional projector, the surface area is a sphere ($4\pi r^2 = 12,6m^2$). Thus,

$$SL_{projector} = 10log((P_{tx}/12,6)/I_{ref}) \quad (dB) \tag{2.6}$$

where P_{tx} is the total acoustic power emitted by the projector. The reference intensity is:

$$I_{ref} = \frac{(Pa_{ref})^2}{\rho c} \quad (Wm^{-2}) \tag{2.7}$$

and for $\rho = 1025kg/m^3$ and $c = 1500m/s$, average values for sea water [9], the equation for the transmitter acoustic source level for an omnidirectional projector can then be written as follows:

$$SL_{projector}(P) = 170.8 + 10\log P_{tx} \quad (dB) \tag{2.8}$$

For the case of a directional projector, then the projector directivity is given by:

$$DI_{tx} = 10\log(\frac{I_{dir}}{I_{omni}}) \quad (dB) \tag{2.9}$$

where I_{omni} is the intensity in the idealized case when energy is spread uniformly in all spherical directions and I_{dir} is the intensity along the direction of the beam pattern being considered. Normally, the direction taken is the one of the main lobe maximum. Directivity can increase the source level by 20 dB [10]. The more general equation for the transmitter acoustic source level ($SL_{projector}$) can be written:

$$SL_{projector}(P,\eta,DI) = 170.8 + 10\log P_{tx} + 10\log \eta_{tx} + DI_{tx} \quad (dB) \tag{2.10}$$

where now is taken into account the efficiency of the projector η_{tx}, to consider the losses associated with the electrical to acoustic conversion, thus reducing the actual SL radiated power by the projector. This efficiency depends of the bandwidth and quality factor of the projector and may vary from 0,2 to 0,7 for a tuned one [10].

2.4 Underwater Channel characteristics

Physical and chemical properties of seawater affect sound propagation. Due to spreading and absorption, an underwater acoustic signal will suffer attenuation. Furthermore, depending on channel geometry, multi-path fading may occur and produce significant inter-symbol-interference (ISI) at the receiver hydrophone. For calculations of the Signal-to-Noise ratio (SNR) or Bit Error Rate (BER) estimation, it is then crucial to understand and establish a good channel model.

2.4.1 Spreading loss

Spreading loss is due to the ever-increasing area covered by the same amount of the sound signal energy, as a wave front moves outward from the source. It is given by

$$PL_{spreading}(r) = k \times 10\log(r) \quad (dB) \tag{2.11}$$

where r is the range in meters and k is the spreading factor.

When the medium in which signal transmission occurs is unbounded, the spreading factor is k=2, meaning that the source intensity decreases with the square of the distance r. In the case of bounded spreading this factor takes different values. For example, k=1 for a cylindrical boundary.

In 1967, Urick suggested that spherical spreading was a rare occurrence in the ocean but recognized that at short ranges it may occur. As Autonomous Underwater Vehicles (AUV) swarm operations and Underwater Sensor Networks (USN) will typically be short range applications, it is likely that spherical spreading will need to be considered the primary factor leading to signal attenuation, in those cases. Spreading loss has a logarithmic relationship with range r and its impact on the signal is most significant at very short range, which is up to approximately 50m. [11]

At these shorter ranges, spreading loss plays a proportionally larger part when compared with the absorption loss, which is the topic of the following subsection.

2.4.2 Absorption loss

The absorption loss represents the energy loss in the form of heat, due to the viscous friction and ionic relaxation that occurs as the sound wave propagates outwards underwater. This loss may be given by the following generic equation:

$$PL_{absorption}(r, f) = 10\log(\alpha(f)) \times r \quad (dB) \tag{2.12}$$

where α is the absorption coefficient that depends on frequency. For a given frequency value, absorption varies linearly with range r in kilometres.

More specifically, the absorption of sound in sea water is caused by three dominant effects, namely: viscosity, ionic relaxation of boric acid and magnesium sulphate ($MgSO_4$) molecules and the relaxation time. The effect of viscosity is significant at the high frequencies above 100 kHz, whereas the ionic relaxation effects of magnesium affect the mid frequency range from 10 kHz up to 100 kHz, and boric acid effects dominate at low frequencies, which go up to a few kHz. In general, the absorption coefficient, α, increases with increasing frequency and decreases as depth increases [12]. Its value is significantly higher for sea water when compared to fresh water, due predominately to the ionic relaxation factor. Extensive measurements of absorption losses over the last half century lead to several empirical formulae which take into account frequency, salinity, temperature, pH, depth and speed of sound. A popular version is Thorp's

expression [13], which is based on his initial investigations in the 60's and has then been converted into metric units considered in equation 2.13. It is valid for frequencies from 100 Hz to 1 MHz and is based on sea water with salinity of 35 ppt (parts per thousand), pH of 8, temp of 4 °C and depth of 0 m (atmospheric pressure) which is assumed but not stated by Thorp.

$$\alpha(f) = \frac{0,11f^2}{1+f^2} + \frac{44f^2}{4100+f^2} + 275x10^{-4}f^2 + 0,0033 \ (dB/km) \tag{2.13}$$

Fisher and Simmons (1977) and others, Francois & Garrison (1982), have proposed other variations for the absorption coefficient. In particular, Fisher and Simmons in the late 70's found the effect on the absorption coefficient associated with the relaxation of boric acid. They provided the following more detailed form for α, which varies with frequency, pressure (depth) and temperature (also valid for 100 Hz to 1 MHz with salinity 35 ppt and acidity 8 pH) [13]:

$$\alpha(f,d,t) = \frac{A_1 f_1 f^2}{f_1^2+f^2} + \frac{A_2 P_2 f_2 f_2^2}{f_1^2+f^2} + A_3 P_3 f^2 \ (dB/km) \tag{2.14}$$

.

In this equation d is depth in meters and t is temperature in °C. The $'A'$ coefficients represent the effects of temperature, while the $'P'$ coefficients represent ocean depth (pressure) and $f1, f2$ represent the relaxation frequencies of Boric acid and ($MgSO_4$) molecules. These terms developed by Fisher and Simmons were also considered more recently by Domingo [12].

Figure 2.5 shows the absorption coefficients in dB/km vs signal frequency for both Thorp, and Fisher and Simmons equations. In general, α increases with increasing frequency for any fixed temperature and depth. Up until around 80kHz, a change in temperature has a more significant effect on α than depth [10], but above these frequencies depth becomes the dominant factor. In any case, Thorp's approximation is quite close to Fisher and Simmons and is clearly more conservative at the frequencies shown. It has been shown that at frequencies above 300kHz Thorp's model predicts lower losses, as it does not take into account the relaxation frequencies found by Fisher and Simmons. If depth and frequency are fixed and temperature varied from 0 to 27°C, there is a decrease in α of approximately 4 dB/km for frequencies in the range of 30 to 60 kHz, which correlates to work presented by Urick [11].

If we consider where AUV swarms are most likely to operate, in the 'mixed surface layer', where temperature varies considerably due to latitude, but with an average value of 17°C, temperature variations may be an important factor. It should be noted that when operating at lower temperatures α will have an higher value and, so, using 0°C will be a conservative alternative. At shorter ranges, the significance of α is expected to be less than spreading loss due to the linear relationship of absorption loss with range.

As mentioned, depth (pressure) has less of an effect on α than temperature at lower frequencies. Domingo investigated the effect of depth (pressure) on absorption and confirmed that for frequencies below $100kHz$ there is less change in α. Urick also studied this variation and proposed the following formula [12]:

$$\alpha_d = \alpha * 10^{-3} d(1 - 5.9 * 10^{-6}) \quad (dB/m) \tag{2.15}$$

where d is depth in meters, but he also suggested as an approximation to take a 2% decrease for every 300 m depth change. Thus, depth (pressure) variations are not expected to play a significant role in short range AUV swarm operations, especially those that use a 2D horizontal topology as described in [11].

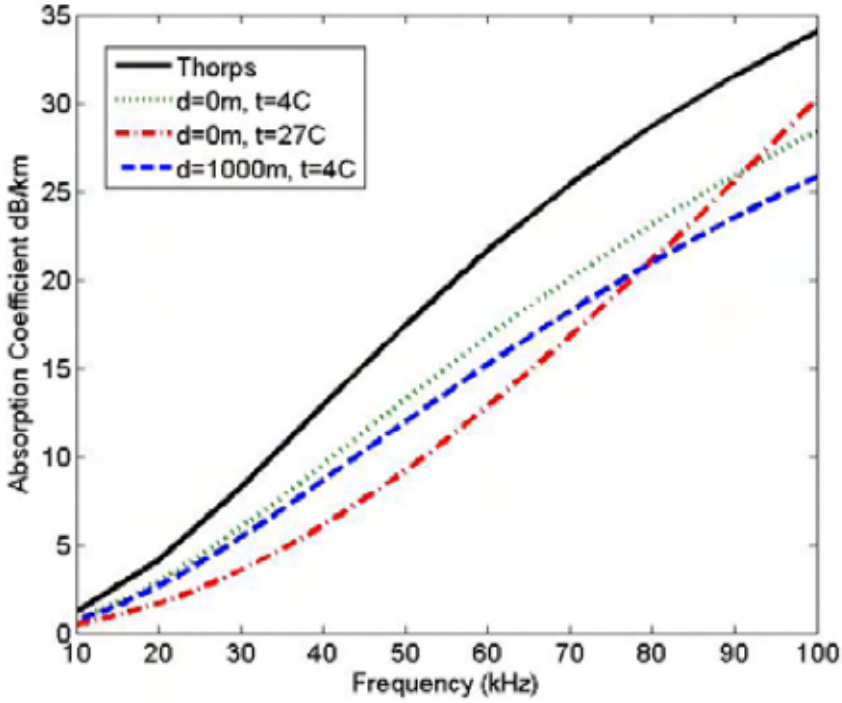

Figure 2.5: Absorption coefficients

2.4.3 Path loss

Total path loss, or just path loss, is the combined contribution of both the spreading and absorption losses. In the year of 1967, Urick established that the formula below, for spreading plus absorption, yields a reasonable agreement with long term observations [11].

$$PathLoss(r,f,d,t) = k.10\log(r) + \alpha(f,d,t).r.10^{-3} \quad (dB) \tag{2.16}$$

2.4.4 Channel bandwidth

The attenuation or path loss that occurs in an underwater acoustic channel for a signal of frequency f and over a distance d may also be given by the following equation:

$$A(l,f) = d^k * a(f)^d \tag{2.17}$$

where k is the spreading factor (typically the value of 1,5 is used), and $a(f)$ is the absorption coefficient. For frequencies above about 100 Hz, as we have seen, the absorption coefficient can be written empirically, using Thorp's formula, which gives $a(f)$ more precisely than other models.

The main limitative factor that cuts the maximal desired range of frequencies usable in an underwater system is the absorption loss coefficient. Raising the frequency, leads to an increase of the path loss due to the increase in the absorption coefficient, turning the frequencies above a certain threshold unusable for acoustic underwater communications. This bandwidth limitations are shown in table 2.2 [10].

Table 2.2: Bandwidth available at different ranges

	Range (km)	Bandwidth (kHz)
Very Long	1000	< 1
Long	10 - 100	2 - 5
Medium	1 - 10	10
Short	0,1 - 1	20 - 50
Very Short	< 0,1	> 100

2.4.5 Noise

For the underwater channel four noise components are considered. There is the thermal noise ($N_{th}(f)$), that can be taken as additive white gaussian noise that is always present in communications systems. Then, there is noise due to the movement of waves ($N_w(f)$), making the water medium unstable and varying the static properties of the channel. Another type of noise is water movement caused by ship traffic ($N_s(f)$) and, finally, theres is also noise due to natural causes ($N_t(f)$), like the turbulence caused by storms or during the rain events and the presence of bubbles. The total noise can be obtained adding of all this contributions as shown by the equations 2.18 to 2.21 (annex B).

$$\text{Turbulence Noise } N_t = 10^{\frac{((17-30\log 10(f))}{10}} N_{t_{Off}} \tag{2.18}$$

$$\text{Shipping Noise } N_s = 10^{\frac{((40+(20(s-0,5))+(26\log 10(f))-(60\log 10(f+0,03)))}{10}} N_{s_{Off}} \tag{2.19}$$

$$\text{Wave Noise } N_w = 10^{\frac{(50+(7,5(\omega^{1/2}))+(20\log 10(f))-(40\log 10(f+0,4)))}{10}} N_{w_{Off}} \tag{2.20}$$

$$\text{Thermal Noise} N_{th} = 10^{\frac{((-15+20\log 10(f))}{10}} N_{th_{Off}} \tag{2.21}$$

$$\text{Total Noise} N = N_t + N_s + N_w + N_{th} \tag{2.22}$$

2.4.6 Propagation delay

The delays experienced in an underwater acoustic communication link are much higher than in an open-air link. The nominal speed of sound in water is $1500 m/s$, which is hundreds times lower than the speed of electromagnetic waves in open-air ($3 \times 10^8 m/s$). This causes long propagation delays, which become a

major complication for applying feedback techniques in correcting the channel distortions. As an example, typical propagation delays in acoustic underwater links can be of several seconds, while the measured coherence time in an underwater channel can be of 100*ms*. In contrast with the propagation delays in underwater channels, the open-air propagation delay is typically of some microseconds [1].

2.4.7 Multipath

Multipath propagation is a common problem in acoustic underwater communication links. This effect results from the fact that several replicas of the transmitted signal reach the receiver after traveling through different paths, with different attenuations and delays. This may lead to severe inter-symbol-interference [14], [15], [16]. In such cases, one may need to use diversity methods or more sophisticated modulation techniques, such as OFDM, in order to obtain an adequate communication [7].

Underwater multipath can be caused either by reflection or refraction of the acoustic waves. Reflection of the acoustic wave occurs when the wave bounces either at the surface or the bottom of the sea and reaches the receiver. It is most common in shallow water environments. Refraction of the waves is a typical phenomenon in deep water links, where the speed of sound changes with depth. An illustrative scheme is shown in figure 2.6:

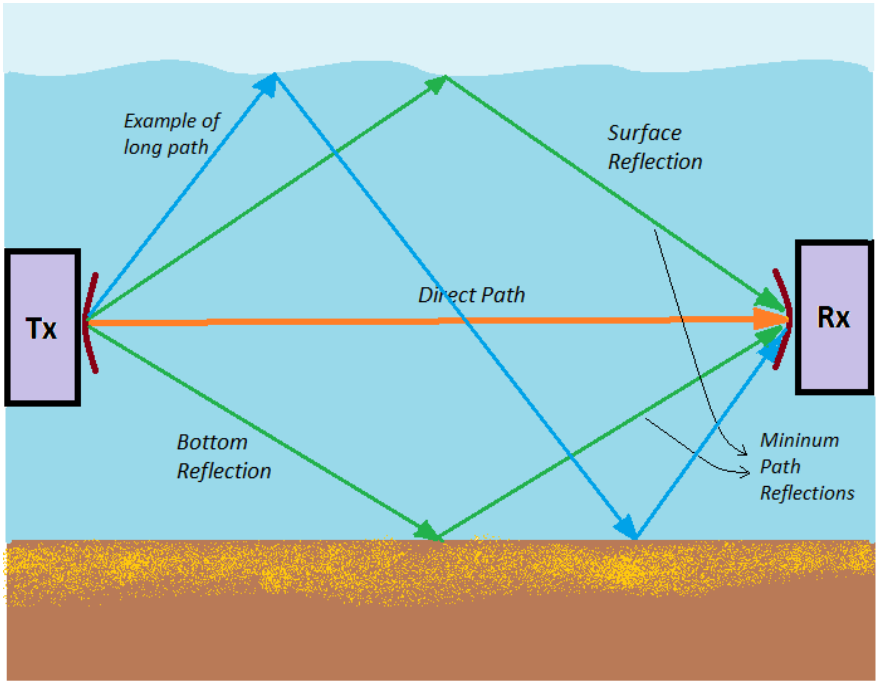

Figure 2.6: Multipath in a transmission

2.4.8 Doppler effect

Doppler effect for short ranges has no relevant effect in underwater communications[1] [5], [6], [17]. The motion of the AUVs relative to each other will cause two possible forms of Doppler distortion in the received signal. Doppler Shifting caused by an apparent shift in frequency, as the vehicles move towards or away from each other, and Doppler Spreading or its time domain dual coherence time, which is the measure of the time varying nature of the frequency dispersiveness in the Doppler spectrum. The Doppler shift (Δf) of a received signal is:

$$f_c = \frac{\Delta v}{c} \tag{2.23}$$

where f_c is the original signal frequency and Δv is the relative velocity between the moving vehicles. As an example, if the vehicles were moving at a moderately slow speed of 1 m/s (2 knots) relative to each other and $f_c = 40kHz$ then $\Delta f \approx 27Hz$. Figure 2.7 illustrates the doppler effect.

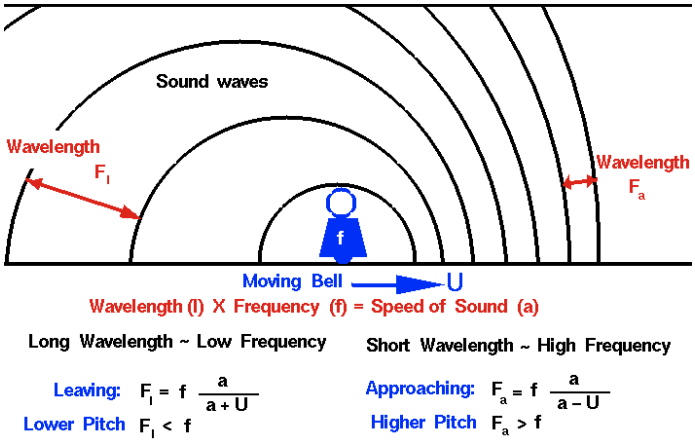

Figure 2.7: Doppler shift

2.5 Research on UWAC

Several research groups are actively working in the UWAC area.

At the Massachussets Institute of Technology, a group leaded by Prof. Milica Stojanovic, has been working in this field, investigating the use of MIMO and OFDM techniques [16] [6] [18]. Also a group from Bremen University of Applied Sciences, has been working in UWAC with emphasis on modelling and simulation of the communication systems [5]. As another example, the Broadband Wireless Network in Lab from the Georgia Institute of Technology, has been working in the topic of underwater acoustic sensor networks (UW-ASN) [14] [19].

Therefore, this field is being studied and relevant advances are expected for the near future.

[1] Based on experiments done on previous work of this project

Chapter 3

Modulation Techniques

The process of systematically modifying a well known deterministic signal, called carrier, in accordance with an information signal is called modulation. This process needs to be reversible, so that the receiver may be able to recover the information signal, via a process called the demodulation. This two-step process of modulation-demodulation is necessary when we cannot transmit the signal directly in its original form through the channel, thus necessitating the translation of the information to another frequency band that suits the channel being used.

3.1 Analog and digital modulations

When the modulating signal is analog, one uses what is known as analog modulations. Conversely, one uses digital modulations when the modulating signal is digital. In either case, the carrier amplitude, frequency, phase or combinations of these three variables, may be altered by the modulating signal. Normally, analog modulation occupies less bandwidth but it is not so robust as digital modulation. The possibility of converting an analog signal to digital using an analogic to digital converter (ADC) and then obtaining the analog signal using a digital to analogic converter (DAC) paved the way to have an all digital network, where all types of services, voice, video, data are integrated [17].

3.1.1 Types of modulation

There is a large number of modulation types, particularly in the digital domain. With the usage of ADC and DAC converters, the number of modulating possibilities increased. The most frequently used modulations for experiments in underwater communications are Multiple Phase Shift Keying (MPSK) and OFDM, mentioned earlier.

In MPSK, each M bits are associated to a symbol, according to a table, and each symbol corresponds to a phase of the carrier (usually, M is a power of two). Then the demodulator has to detect the different

phases received sequentially, thus recovering the different symbols and, ultimately, the bits associated with each symbol [20].

In OFDM, a set of mutually-orthogonal frequencies is used and to each frequency a digital modulation, like BPSK, is applied. The advantages of OFDM are: to adapt to severe channel conditions without having to use complex equalization filters; robustness against intersymbol interference and the usage of the efficient FFT technique. On the down side, OFDM is sensitive to the Doppler effect, frequency synchronization problems and presents some efficiency loss due to the use of the cyclic prefix (interval of guard) necessary to combat multipath problems [21], [22], [23].

3.2 Analog modulations

Given that analog modulations are not used in the present work, we present only a very brief review of the basic principles. In these modulations the carrier is a sinusoidal signal and its amplitude, phase or frequency may vary proportionally to the message signal. Therefore we can have Amplitude Modulation (AM), as shown in figure 3.1 for the conventional case, and we can have Phase Modulation (PM) and Frequency Modulation, as shown in figure 3.2 for the simple case of a sinusoidal modulating signal.

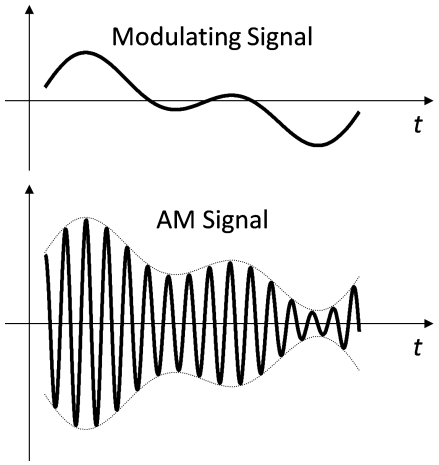

Figure 3.1: Conventional AM modulation

3.3 Digital modulations

In this section is presented a review on digital modulations, considering first the case when the modulating signal is a binary waveform. The most relevant binary digital modulations are then detailed, followed by the case when the symbols used represent more than two bits and the more important M-ary digital modulations.

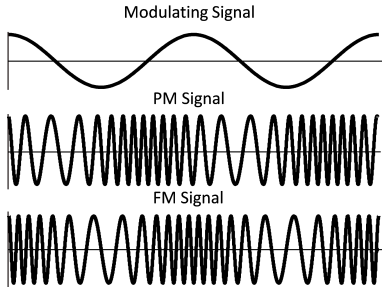

Figure 3.2: Conventional PM and FM modulations

3.3.1 Binary modulations

Figure 3.3 shows the waveforms of a carrier when its amplitude (Amplitude Shift Keying - ASK), phase (Phase Shift Keying - PSK) or frequency (Frequency Shift Keying - FSK) are changed according to the binary message to be transmitted.

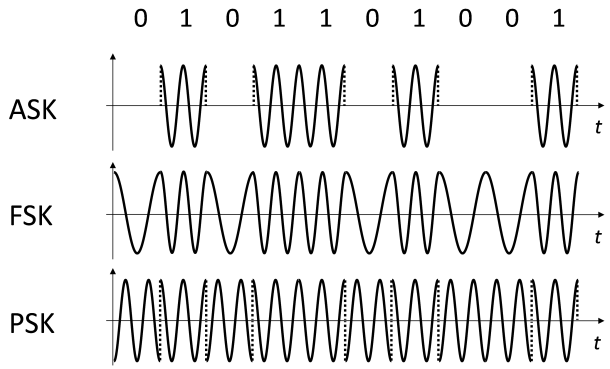

Figure 3.3: Waveforms for the simplest binary digital modulations

The case shown for ASK is normally called On-Off Keying (OOK) since no carrier is transmitted for the duration of the binary 0-symbols, with the effect that the carrier is only turned on for the duration of the binary 1-symbols. In the following we adopt an orthonormal signal space analysis [17] [24] [25] given that this geometric representation of signals offers a common base to analyze all digital modulation types.

3.3.1.1 Binary Phase Shift Keying (BPSK)

A BPSK signal is defined by the following equations:

$$\begin{cases} s_1(t) = \sqrt{(\frac{2E_b}{T_b})}\cos(\omega_c t + \theta)(\theta = 0) \\ s_2(t) = \sqrt{(\frac{2E_b}{T_b})}\cos(\omega_c t + \theta + \pi) = -s_1(t) \end{cases} \quad 0 \leqslant t \leqslant T_b \tag{3.1}$$

where T_b is the bit duration, E_b is the bit energy, ω_c is the angular frequency ($\omega_c = 2\pi f_c$ where f_c is the frequency of the carrier) and θ is the initial phase that may be taken equal to zero. The equation clearly shows that the constant phases used to represent each symbol are separated by π. For this modulation, in an orthonormal signal space, only one basis function is needed and it is given by

$$\Psi_1(t) = \sqrt{\frac{2}{T_b}}\cos(\omega_c t) \tag{3.2}$$

Figure 3.4 shows the constellation for the BPSK signal and the expression for determining the Bit Error Rate (BER) when an Additive White Gaussian Noise (AWGN) is assumed. The BER expression uses the q-function to obtain the needed area under the Gaussian curve and N_o represents the power spectral density of the white noise. Note that, for a given noise level, the BER is a function of the distance d between the two constellation points associated to the two binary symbols.

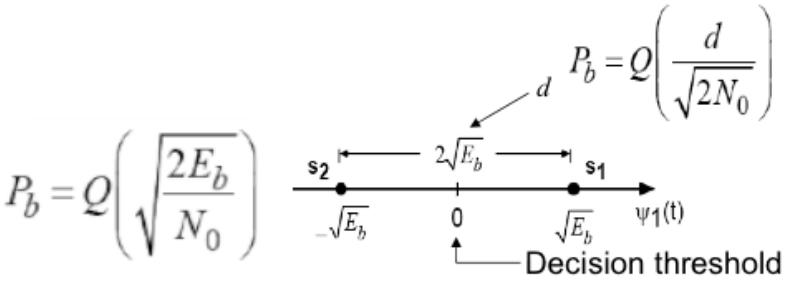

Figure 3.4: BPSK constellation and BER expression

Demodulation of a BPSK signal must be done with a coherent detector meaning that at the receiver one needs the same frequency and phase of the BPSK carrier transmitted. This may lead to more complex receivers. Alternatively, Differential PSK (DPSK) may be used, avoiding the problem of recovering the carrier frequency and phase but at the expense of higher BER.

3.3.1.2 Binary Frequency Shift Keying

A BFSK signal is given by the following equation

$$s_i(t) = \sqrt{\frac{2E_b}{T_b}}\cos 2\pi f_i t = \sqrt{\frac{2E_b}{T_b}}\cos(2\pi f_c t \pm \frac{\pi}{T_b}t) \quad \begin{matrix} 0 \le t \le T_b \\ i = 1,2 \end{matrix} \tag{3.3}$$

meaning that two different frequencies are used and each one for a corresponding binary symbol. Normally the relation between these two frequencies is:

$$f_1 = f_c - \frac{1}{2T_b} \tag{3.4}$$

$$f_2 = f_c + \frac{1}{2T_b} \tag{3.5}$$

so the two signals $s_i(t)$ are orthogonal and also have phase continuity. This case is known as Continuous Phase FSK (CPFSK) and is shown in figure 3.5.

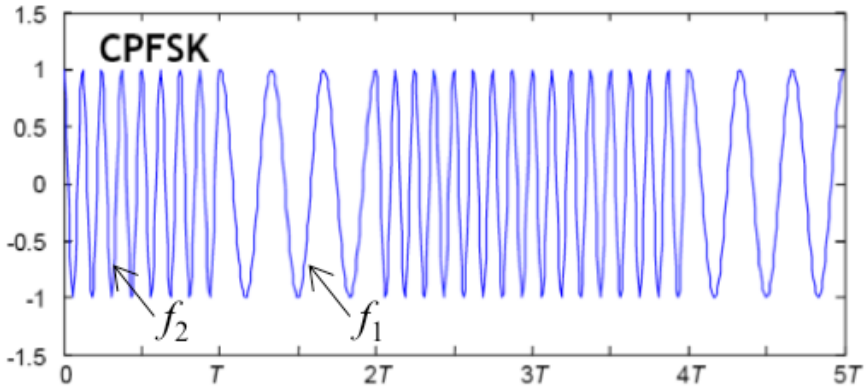

Figure 3.5: Binary CPFSK waveform

In the signal space we require now two base functions to represent the BFSK signal, as is shown in figure 3.6, where the BER expression is also presented. Note that the distance between the constellation points in BFSK is less than in BPSK so that, given the same $\frac{E_b}{N_o}$ value, the BER obtained is worse for BFSK.

$$P_b = Q\left(\frac{d}{\sqrt{2N_0}}\right) = Q\left(\sqrt{\frac{E_b}{N_0}}\right)$$

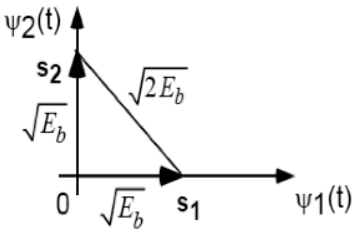

Figure 3.6: BFSK constellation and BER expression

At the receiver side, BFSK can use either a coherent detector or a non-coherent detector. In this last case the receiver is simplified but the BER performance deteriorates.

3.3.1.3 Binary Amplitude Shift Keying

The Binary Amplitude Shift Keying (BASK) signal normally used is the OOK signal. This, in turn, may be viewed as a BPSK signal where one of the symbols, normally symbol zero, turns off the carrier. As a

consequence, the carrier is only sent when the other symbol occurs. Given these facts, from figure 3.4 we immediately conclude that OOK constellation has one point at $\sqrt{(E_b)}$ and the other at the origin. Therefore the BER obtained will be worse than in BPSK and, it can be shown [17], [24] that coherent OOK has the same BER performance as coherent BFSK. The OOK receiver may be coherent, as stated above, but normally a non-coherent receiver is used, with a simple envelope detector, with some degradation of the resulting BER.

3.3.1.4 Comparison of the binary digital modulations BER

Figure 3.7 presents a summary, showing digital communications relative BER performance, as a function of $\frac{E_b}{N_o}$.

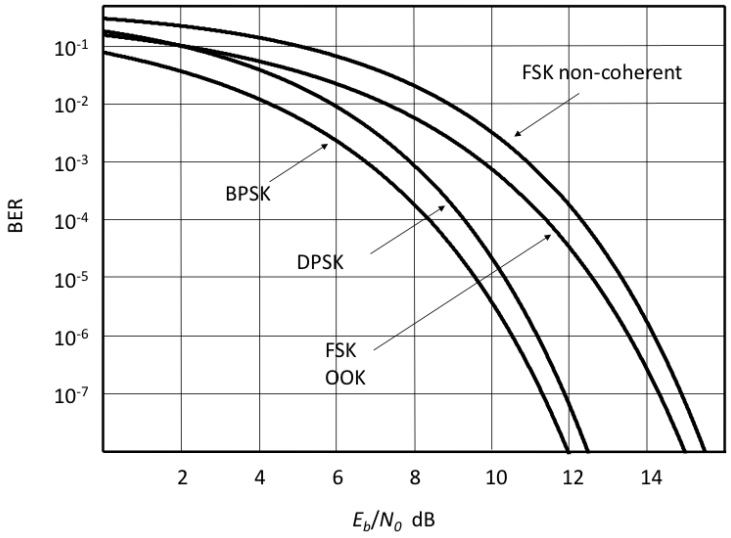

Figure 3.7: BER performance of binary digital modulations

To conclude this brief presentation, an interesting experimental tool that also enables BER and ISI evaluation is the eye pattern. It is obtained by the synchronized superposition of all received symbols during the timespan of one symbol. The information that can be extracted from the eye pattern, regarding the communication performance, is shown in figure 3.8.

3.3.2 *M*-ary modulations

In the M-ary modulation techniques, each symbol represents a fixed number of bits n_b. Usually, M is chosen to be a power of two, so that the relation $n_b = \log_2 M$ holds and the symbol duration is $T_s = n_b T_b$, where T_b is the bit time duration. For all M-ary modulations, at the modulator there is a first step where serial to parallel conversion takes place, to go from bits to their symbol representation. On the other end of

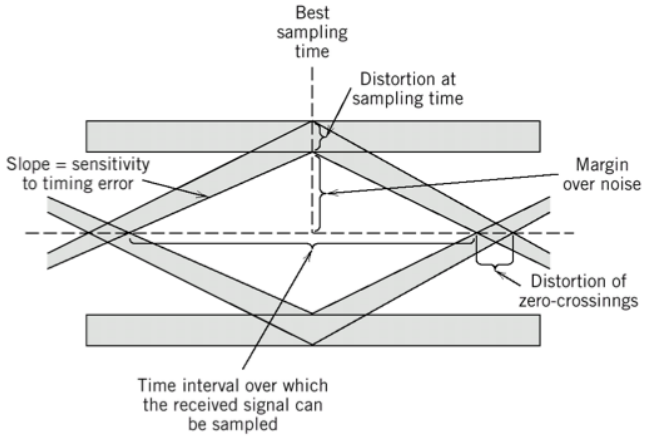

Figure 3.8: Interpretation of the eye pattern

the process, at the demodulator, the final step must be a parallel to serial conversion, in order to obtain the bit stream from the detected symbols. In the following sections the most relevant M-ary modulations are presented.

3.3.2.1 M-ary Phase Shift Keying

In M-ary Phase Shift Keying (MPSK) to each symbol corresponds a phase of the carrier and the M phases are equally spaced over 2π. Figure 3.9 shows the constellation for the case of a MPSK signal with $M = 8$.

Note that two base functions are necessary to draw the signal constellation and the decision boundaries are determined as shown in the figure. The expression for the probability of error, also presented in the figure, corresponds to the symbol error probability and it should be divided by $3 = \log_2 8$, if we consider that errors occur only to the closest neighbours and that Gray encoding is used [17] [25]. A particular but very important case of MPSK arises when $M = 4$ and each symbol represents two bits. This case has the particular name of QuadriPhase Shift Keying (QPSK), and corresponds also to a quadrature amplitude modulated signal with $M = 4$ (see next subsection). A QPSK signal is given by the following equation:

$$s_i(t) = \sqrt{\frac{2E}{T_s}} \cos\left(2\pi f_c t - (2i-1)\frac{\pi}{4}\right) \quad \begin{matrix} 0 \le t \le T \\ i = 1,2,3,4 \end{matrix} \quad f_c = n_c \frac{1}{T_s} \tag{3.6}$$

and its constellation is shown in figure 3.10, where the symbol regions are the four quadrants and a possible Gray encoding is also shown.

This modulation may also be viewed as two orthogonal BPSK signals and the BER obtained for the QPSK case is the same as for the BPSK case, with the advantage that, for the same bandwidth, we can double the transmitted bit rate in the QPSK case [17] [24].

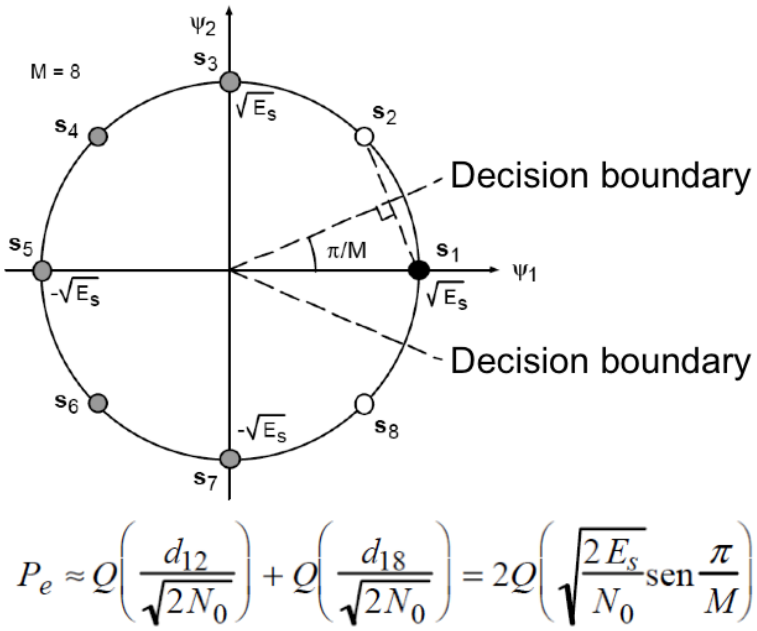

Figure 3.9: 8PSK constellation and symbol error probability expression

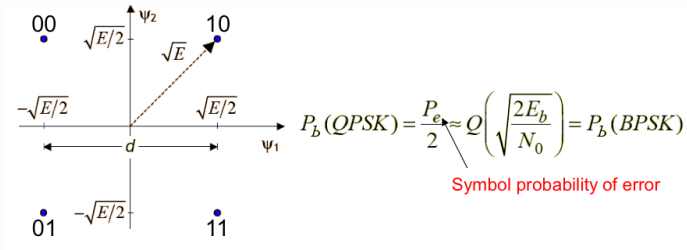

Figure 3.10: QPSK constellation and BER relation with BPSK case

3.3.2.2 *M*-ary Quadrature Amplitude Modulation

M-ary quadrature amplitude modulation is a hybrid case of phase and amplitude modulation where usually square constellations are used. The QAM signal may be expressed by the following equation:

$$s_i(t) = \sqrt{\frac{2E}{T_s}}\cos\left(2\pi f_c t - (2i-1)\frac{\pi}{4}\right) \quad \begin{array}{l} 0 \le t \le T_s \\ i = -L+1, ..., -1, 0, 1, ..., L-1 \end{array} \tag{3.7}$$

where a_i and b_i are the possible coefficients used in the in-phase and quadrature components, and $L = \sqrt{M}$. Figure 3.11 shows a constellation for a 16QAM signal with a possible Gray encoding and the BER expression [17], [25]. As stated above the case 4QAM corresponds to the QPSK modulation.

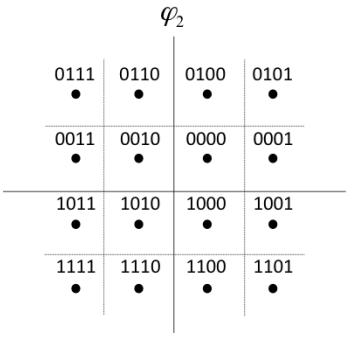

$$P_b \approx \frac{4(1-\frac{1}{\sqrt{M}})}{\log_2 M} Q\left(\sqrt{\frac{3\log_2 M}{M-1}\frac{E_b}{N_0}}\right)$$

Figure 3.11: 16QAM constellation and BER expression

3.3.2.3 Comparison of *M*-ary digital modulations BER

As it was done in section 3.3.1.4, we now present in figure 3.12 a comparison on the relative performances of *M*-ary digital modulations, regarding the BER obtained as a function of E_b/N_o. BPSK is also included in order to have a reference term to compare with figure 3.7.

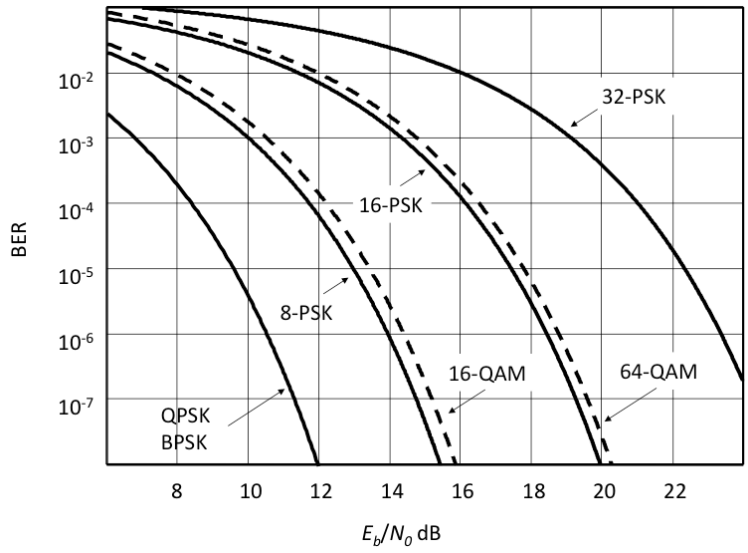

Figure 3.12: BER performance of *M*-ary digital modulations

3.3.2.4 *M*-ary Frequency Shift Keying

In *M*-ary Frequency Shift Keying (MFSK) there M orthogonal base functions, the *M* carriers used in this modulation type being mutually orthogonal for the duration of the symbol. This implies that the constellation

spans an M-dimensional orthonormal space. The following equations describe an MFSK signal and the orthogonality relation between the carriers

$$s_i(t) = \sqrt{\frac{2E}{T_S}} \cos\left[\frac{\pi}{T_s}(n_c + i)t\right] \; 0 \le t \le T_s \, i = 0, 1, 2, ..., M \, f_c = \frac{n_c}{2T_s} \tag{3.8}$$

$$\int_0^T s_i(t) s_j(t) dt = 0 \, i \neq j \tag{3.9}$$

Figure 3.13 shows the symbol error probability bound for MFSK [24] [25] and the corresponding BER.

$$P_e \le (M-1)Q\left(\sqrt{\frac{E_s}{N_0}}\right)$$

$$P_b = \frac{2^{k-1}}{2^k - 1} P_e \quad \text{with} \quad k = \log_2 M$$

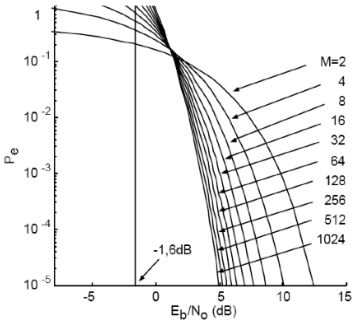

Figure 3.13: BER Performance of MFSK modulation

Notice that for values of P_e in the area of usual interest (for example below 10^{-3}) there is a decrease in E_b/N_o with the number of carriers used to reach the same P_e value, but this benefit approaches a limit as seen in the figure.

3.3.3 Bandwidth Efficiency

For completeness, in this brief review of digital modulations, it is important to compare the bandwidth requirements of the various digital modulation schemes. This may be done by looking directly at the bandwidths B, which depend on the bit rate R_b, or by looking at the modulation efficiencies ε as it is shown in table 3.1.

Table 3.1: Bandwidth B and efficiency ε for various modulation types

Modulation	Nominal Values		Optimum Values	
	B	ε	B	ε
MPSK and M-QAM	$\frac{2R_b}{\log_2 M}$	$\frac{\log_2 M}{2}$	$\frac{R_b}{\log_2 M}$	$\log_2 M$
MFSK (coherent det.)	$\frac{M+3}{2\log_2 M} R_b$	$\frac{2R_b}{\log_2 M}$	$\frac{M+3}{2\log_2 M} R_b$	$\frac{2\log_2 M}{M+1}$
MFSK (non-coherent det.)	$\frac{M+1}{\log M} R_b$	$\frac{\log_2 M}{M+1}$	$\frac{M}{\log M} R_b$	$\frac{\log_2 M}{M}$

3.3.4 Orthogonal Frequency Division Multiplexing

The water channel that is being considered in this thesis may have multipath effects. The modulations so far described suffer a lot in such an environment and multipath may even impair the communication to a level where the message becomes unrecoverable. With this in mind, it is important to look at more robust modulations when multipath effects are present. Nowadays, OFDM is considered always as a strong candidate to use in such cases. The basic idea of OFDM is to divide the available usable spectrum into many narrowband, low data rate carriers, called subcarriers. Each narrowband orthogonal subcarrier can be modulated using various modulation formats, BPSK, QPSK and QAM being commonly used. Subcarrier spacing is chosen sufficiently close so that the channel transfer function may be approximated by a constant complex value within the bandwidth used by each subcarrier. In this way, a frequency selective channel is divided into many flat fading sub-channels where each subcarrier suffers only constant phase and amplitude changes. The OFDM signal lasts a long time in the channel that, by project, must exceed the time span where multipath effects take place. A cyclic prefix, which is basically a copy of the last part of the OFDM symbol, is added at the beginning of each OFDM symbol exactly where the multipath will have impact. Then, the remaining part of the symbol is free from multipath as shown in figure 3.14.

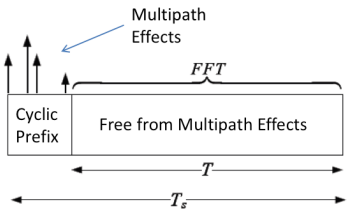

Figure 3.14: OFDM basic principle for avoiding multipath effects

A block diagram of the OFDM system is shown in figure 3.15 [26]. Clearly this system may be rather complex but offers great performance when multipath is a problem.

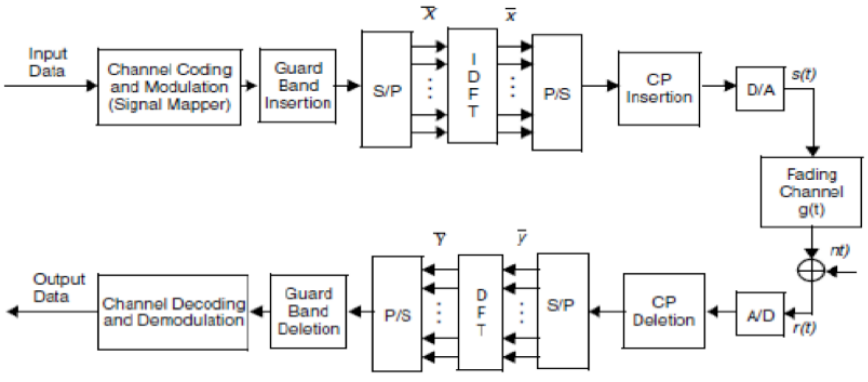

Figure 3.15: OFDM system block diagram

In the first block, codification and modulation of data is done. On the second, is added a guard band in each data frame and a convertion from serial transmission to paralell is done in the follow block. In paralell format, inverse discrete Fourier transform operation is applied to the data and converted again from paralell to serial. Then a ciclic prefix is concatenated in the signal and for last a conversion from digital to analog format is done. This is the process realized before the transmission to the medium is accomplished. Since this is a simulation model, there is a block simulating the fading channel with noise adding and then occurs the reverse process in the receiver end, where the same blocks with the reverse function, recovers the data.

Chapter 4

UWAC Project

This project was designed and started at the *Universidade do Minho* to explore an emerging field of communications, that is, the UWAC.

The project covers several areas, such as acoustic, signal processing, communication techniques and power supplying. The aim is to develop an UWAC system with a significant bit rate capacity, able not only to transmit telemetry and control signals but also images and video signals.

4.1 UWAC set-up at *Universidade do Minho*

In this section we describe briefly the equipment available at *U.M.* for the UWAC project, that are used in the ongoing experimental work.

4.1.1 Projectors and Hydrophones

Transducers are devices that convert some sort of energy into another. For example, we may have optical transducers that convert optical signals into electrical signals and vice-versa. For the present work, acoustic transducers are relevant and they are called projectors (perform the conversion of electrical signals to acoustic underwater waves) and hydrophones (conversion of acoustic underwater waves to electrical waves).

The two main projectors used for underwater communications are the one with *Lead Zirconate Titanate* inorganic compound (PZT), and the other with *PolyVinyliDene Fluoride* (PVDF).

The PZT projector has this name since it uses a piezoelectric ceramic, made with *Lead Zirconate Titanate*. This material shows a marked piezoelectric effect, which finds practical applications in the area of electroceramics and may be used as a projector [1].

The PVDF projector uses a piezoelectric polymer made with *Polyvinylidene Fluoride*, or *polyvinylidene Difluoride Lead*. PVDF is used, in general, in applications that require high levels of purity, strength, and

resistance to solvents, acids, bases and heat. It also generates low smoke quantities in a fire accident. Data sheets are not presented since the equipments is not the focus of this work [1].

Figure 4.1 shows both the projector and the hydrophone used at UM.

Figure 4.1: Projector and hydrophone

4.1.2 Amplifiers

In order to condition the signal power levels at the transmitter and at the receiver, amplifiers were used at both ends. Figure 4.2 shows on the left the transmitter amplifier whose purpose is to drive the projector with an adequate power level. On the right of the figure 4.2, there is an image of the receiver amplifier used, whose function is to produce at its output electrical signal levels that can be conveniently used by the following receiver hardware. Data sheets of these two amplifiers are not presented, due to the same reason given above.

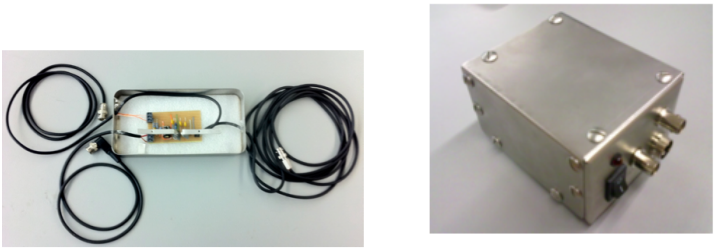

Figure 4.2: Transmitter Receiver amplifiers

4.1.3 Signal generator

In many practical situations, like real world tests, for example, it is desirable to have the possibility of using well known signals with various different waveforms such as sinusoidal, sawtooth, impulse and square wave. One needs also to be able to change certain parameters of these signals, like frequency and amplitude. All this can be done using a signal generator, like the one shown in figure 4.3, used in this project.

Figure 4.3: Signal generator

4.1.4 Picoscope

PicoScope is an equipment that enables the acquisition of signals, using probes similar to the ones used in traditional oscilloscopes, and then a software application which runs on the PC, enabling the displaying and processing of the waveforms acquired.

This equipment, together with the software in the PC, is a very interesting tool due to its low cost and powerful capabilities for displaying, recording and processing a wide range of signals in time domain and even in frequency domain, where it can be used as a spectrum analyzer. Note also that, for the signals used in this work, there is no necessity of a large bandwidth equipment.

Figure 4.4 shows an image of the picoscope used in the project.

Figure 4.4: Picoscope

4.1.5 FPGAs

Field Programmable Gate Arrays (FPGAs) are semiconductor devices that are based around a matrix of Configurable Logic Blocks (CLBs) connected via programmable interconnects. FPGAs can be reprogrammed to the desired application or functionality requirements. Due to their re-programmable nature, FPGAs are ideal for the development phase of the hardware. At *UM* Xilinx FPGAs are used to develop modules for the transmitter and receiver, thus enabling a quick deployment of the hardware for UWAC tests, an example being shown on figure 4.5.

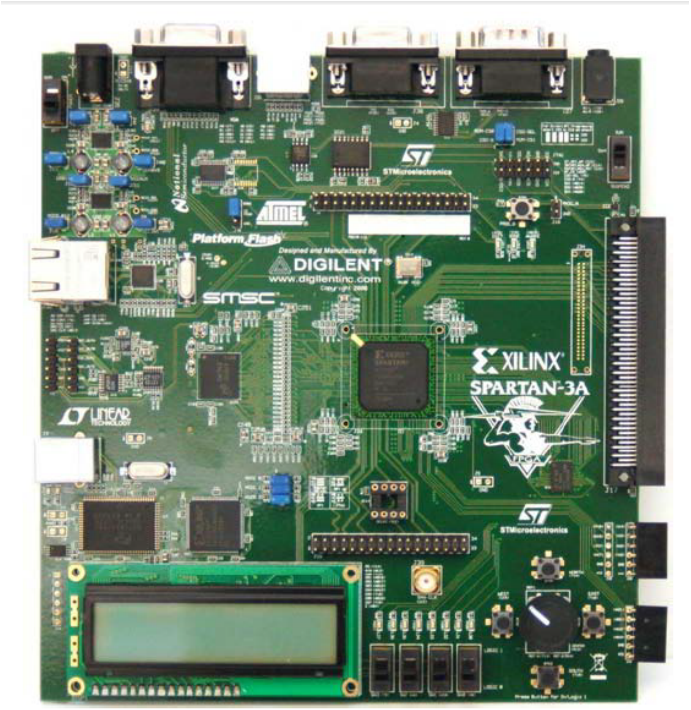

Figure 4.5: FPGA device used at *Universidade do Minho* for the UWAC project

4.2 System model

Figure 4.6 presents the system block diagram, describing the relevant functions that have to be implemented both at the transmitter and receiver and including also a block for the aquatic channel. A software implementation of this system is being developed, to be able to run simulations and compare or predict the system's behavior. The software tool used was MatLab/Simulink and this choice will be explained later on in this chapter.

4.3 Aquatic chanel model

As stated before, present work focuses on the aquatic channel software model for verification with real-world measurements. It is also intended to simulate and compare the performance of some digital modulations that might be used in the UWAC system. Figure 4.7 shows the aquatic channel block breakdown in several internal blocks, which will be discussed in the following subsections. The code for some blocks

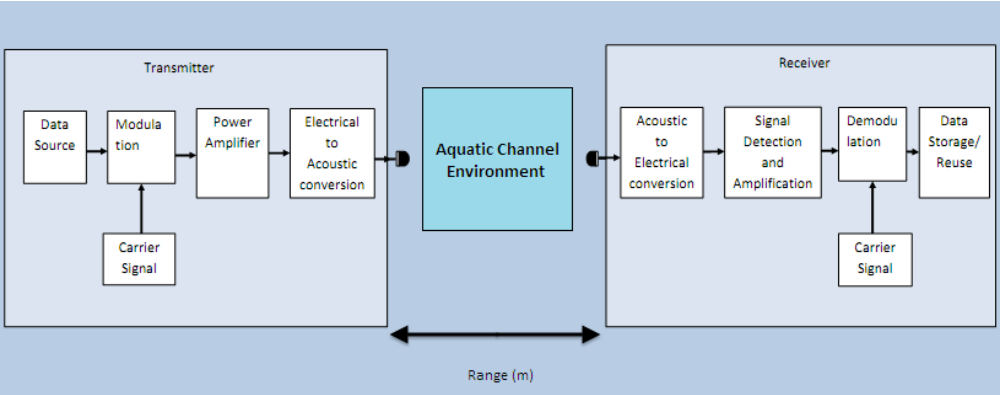

Figure 4.6: System block diagram and the aquatic block model

already existed but had to be altered, particularly due to the insertion of a new block developed that deals with multipath.

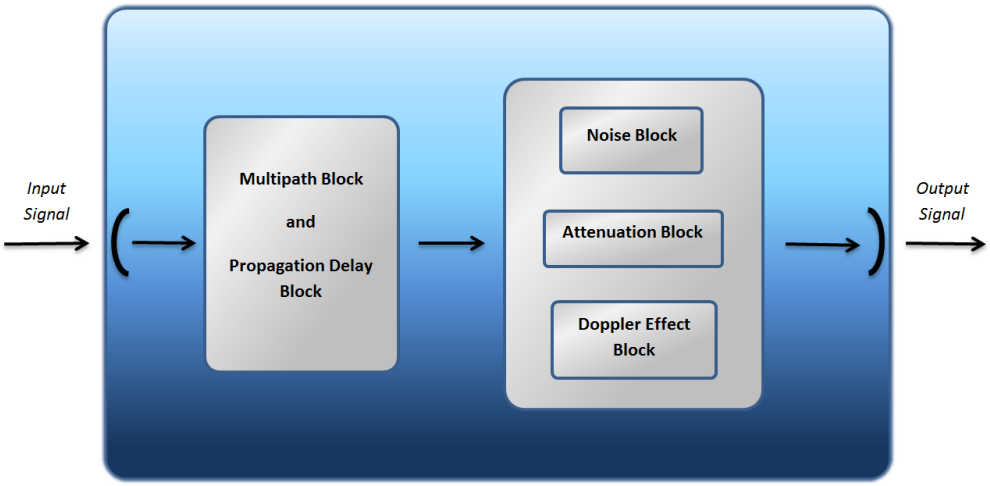

Figure 4.7: Aquatic block model

4.3.1 Attenuation block

The attenuation block implements the attenuation formula already mentioned in Chapter 2.4.3, that determines the loss that the signal suffers while passing the water channel. In a multipath situation, the different path losses are determined. The MatLab code for this block is presented in annex B.

4.3.2 Noise block

In the noise block the various noise contributions, corresponding to equations 2.18 to 2.21 are calculated and added, to obtain the total noise due to the channel. MatLab code for this block is also presented in annex B.

4.3.3 Doppler effect block

This block was considered in order to have a complete description of the channel but was disabled since it was verified that the doppler shift effect was irrelevant for the tests considered in this phase of the project, since the projector and the hydrophone will be placed at fixed positions.

4.3.4 Propagation delay block

This block outputs the signal time delay due to the propagation, from the projector to the hydrophone, inside the water channel. In a multipath case the delays for the various paths with reference to the direct path are determined. The corresponding code is shown in annex B, too.

4.4 The multipath block

Looking back to figure 4.7 we can see that there is a multipath block in the channel that has not been considered yet. Since this was one of the major contributions of the present work, an entire section of this chapter is now devoted to detailing this block.

4.4.1 Multipath Channel Transfer Function

For the multipath case the channel transfer function is given by equation 4.1, with the corresponding impulse response given by equation 4.2.

$$H(f) = \sum_{e=0}^{E-1} \frac{\Gamma_e}{\sqrt{(A(l_e,f))}} e^{-2j\pi f \tau_e} \tag{4.1}$$

$$h(t) = \sum_{e=0}^{E-1} \frac{\Gamma_e}{\sqrt{(A(l_e,f))}} \delta(t-\tau_e) \tag{4.2}$$

In these equations E paths are considered, including the direct one. Each path has its own attenuation and delay values. These, in turn, depend on the distance traveled by each path. All paths contribute for the signal received and may cause significant ISI.

4.4.2 Equations for multipath calculation

To determine the attenuations and delays for each path, including the direct one, we are going to consider ray theory and assume total reflection in the boundaries. From all the possible paths only the ones that have a single reflection are going to be considered since they yield the minimum distances.

Figure 4.8 shows the scheme of the aquarium used on tests. Both transducers are located close to the side walls and are misaligned. Two total reflection paths on the top and bottom walls are shown in the figure as an example. Obviously, besides the direct path, reflections on all six boundaries have to be calculated. In an actual case, given the directivity of the projector and hydrophone, it may happen that some paths can be neglected, as their corresponding signals are in spatial directions where the radiation pattern of the projector, hydrophone or both insert a large attenuation. The width of aquarium was in the x axys, the lenght in the y axys, the depth in the z axys and these dimensions are represented by the constants W, L and D, respectively. The direction of z coordinate axis was inverted with the origin of the axes at an apex of the aquarium floor.

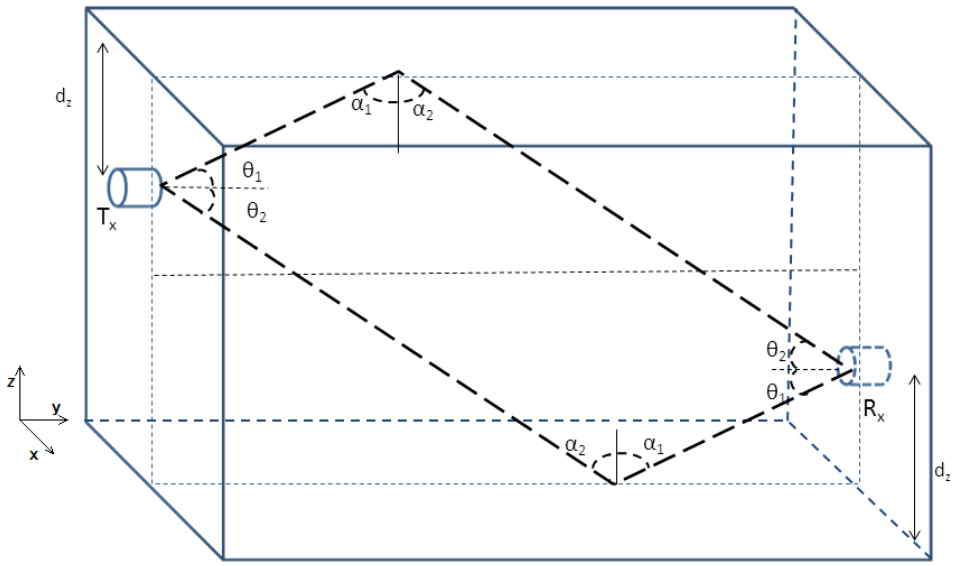

Figure 4.8: Aquarious for test purposes

Taking in consideration the aquarium physical dimensions, the equations 4.3 to 4.15 determine the direct path distance and the six minimum paths distances for the reflections in six plane boundaries, top and bottom walls, two vertical side walls and left and right side walls.

$$
\begin{aligned}
D_1 &= \sqrt{(x_2-x_1)^2+(y_2-y_1)^2+(z_2-z_1)^2} && (4.3)\\
R_{x_{c_2}} &= [2*w-x_2, y2, z2] && (4.4)\\
D_2 &= \sqrt{((2*w-x_2)-x_1)^2+(y_2-y_1)^2+(z_2-z_1)^2} && (4.5)\\
R_{x_{c_3}} &= [-x_2, y_2, z_2] && (4.6)\\
D_3 &= \sqrt{(-x_2-x_1)^2+(y_2-y_1)^2+(z_2-z_1)^2} && (4.7)\\
R_{x_{c_4}} &= [x_2, y_2, 2*D-z_2] && (4.8)\\
D_4 &= \sqrt{(x_2-x_1)^2+(y_2-y_1)^2+((2*D-z_2)-z_1)^2} && (4.9)\\
R_{x_{c_5}} &= [x_2, y_2, -z_2] && (4.10)\\
D_5 &= \sqrt{(x_2-x_1)^2+(y_2-y_1)^2+(-z_2-z_1)^2} && (4.11)\\
R_{x_{c_6}} &= [x_2, -y_2, z_2] && (4.12)\\
D_4 &= \sqrt{(x_2-x_1)^2+(-y_2-y_1)^2+(z_2-z_1)^2} && (4.13)\\
R_{x_{c_7}} &= [x_2, 2*L-y_2, z_2] && (4.14)\\
D_5 &= \sqrt{(x_2-x_1)^2+((2*L-y_2)-y_1)^2+(z_2-z_1)^2} && (4.15)
\end{aligned}
$$

This derivation was made considering reflection law, neglecting the losses in the boundaries and using image sources, which greatly simplified the path distances calculations. The position of the image source is shown in the equation previous to its path distance calculation. Other cases that may help clarifying the calculations are presented in annex A.

4.5 Software tool used for the simulations

MatLab/Simulink was the tool chosen to develop all the simulation models. This tool offers great versatility, both in the time and the frequency domains, with a variety of ready-to-use blocks, which greatly simplifies and speeds up the software development process.

This tool was already being used in the project and there was no reason to change. On the contrary, it is possible to use MatLab/Simulink with the Xilinx System Generator for the DSP tool, in order to quickly create FPGA implementations, even with complex DSP algorithms. This was one of the main reasons why this tool was chosen in the beginning of the project, given that Xilinx FPGAs are used.

4.6 Extra Tasks

Implementation of the channel model, including multipath, was the main objective but other tasks were also performed and some are worth mentioning. Modulations were studied with considerable detail and also a Graphical User Interface (GUI) was developed.

4.6.1 OFDM experiments

After investigating the modulation possibilities, and particularly because of the multipath problem, it was concluded that a highly sophisticated modulation technique, like OFDM, may have to be used to combat the multipath effects. This modulation was studied and MatLab/Simulink models were exploited to evaluate its robustness in a multipath environment for an acoustic underwater communication system. Some preliminary results are shown in annex D. Figure 4.9 shows the multipath effect in a BPSK constellation.

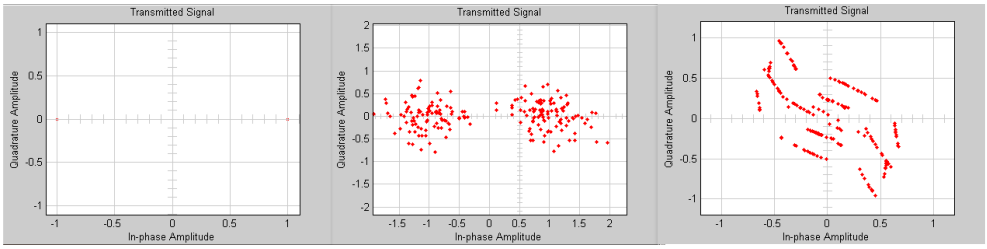

Figure 4.9: Rayleygh multipath UWAC model with BPSK

4.6.2 Graphical User Interface application

The GUI implemented greatly help visualize the multipath phenomenon for the case under study. The first button in the GUI plots a 2D wave propagation visualization (see figure 4.10) from a monopole source, which imitates a omnidirectional projector. There is a slider that enables the user to change the angle of aperture of the acoustic beam propagated from the projector. The second button plots a 3D graph of the same projector and the angle slider has the same function.

The third button, when activated, shows a visualization of the aquarium used for the experimental tests (see figure 4.11). The direct path, or line of sight (LOS), and the four minimum path reflections are traced and red dots are shown where the rays touch the boundaries.

For all the visualizations it is expected that the dimensions of the tank, the coordinates of both transmitter and receiver and aperture angles be defined by the user or some may be defined and other may be calculated or defaulted by the application. Other examples of the GUI are presented in annex C.

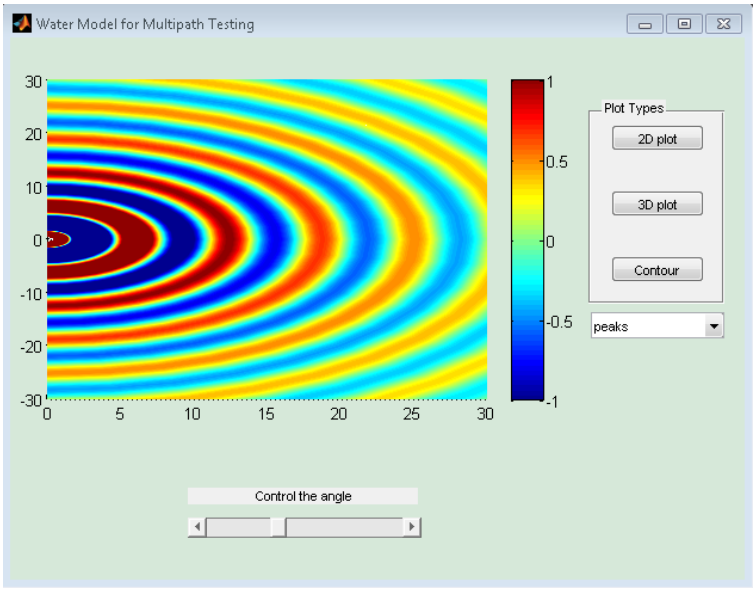

Figure 4.10: 2D Source plot beam pattern

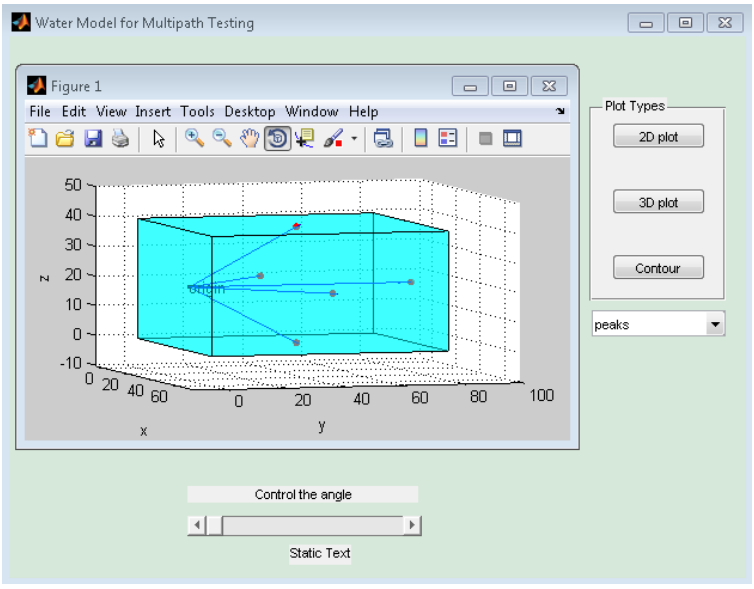

Figure 4.11: Multipath in MatLab GUI application

Chapter 5

Simulations and results

In this chapter are presented the simulation results that were obtained. First, the channel model is considered, focusing on the path loss, and then several modulations are tried out for the aquarium scenario presented in chapter 4. In the later situation, the multipath block is used and it is expected that this enhancement will have considerable impact on the communication system.

5.1 Path loss

As it was shown in chapter 2, the path loss or attenuation is the sum of the spreading loss with the absorption loss, when all these quantities are expressed in dB. Figure 5.1 shows, on the 3D graph at the top left-side, the water channel attenuation dependence of frequency and of the distance from the acoustic source. For the distance, it was considered the range that one expects will be covered by the undergoing project, while for the frequency it was used the range of interest that is normally considered in UWAC. The other two 3D graphs depict the contributions to the attenuation related to the spreading and absorption factors. Notice that spreading is always the dominant source of attenuation, for the range of distances and frequencies covered, but there is a considerable increment in absorption for the high frequency range, close to $1MHz$.

Figure 5.2 presents the absorption coefficient dependence of frequency and figure 5.3 shows the four terms mentioned in chapter 2 are considered. Notice that only one of the terms dominates in the higher frequencies of interest, while, for lower frequencies, all four terms have similar minimal effects and so can be neglected, when compared to the spreading.

5.2 Binary digital modulations simulated and results

The frequency chosen for the optimization of the projector already developed was $1MHz$, since this is the optimal value referred in the UWAC literature and it will be the value used during the physical tests

Figure 5.1: Attenuation, spreading and absorption

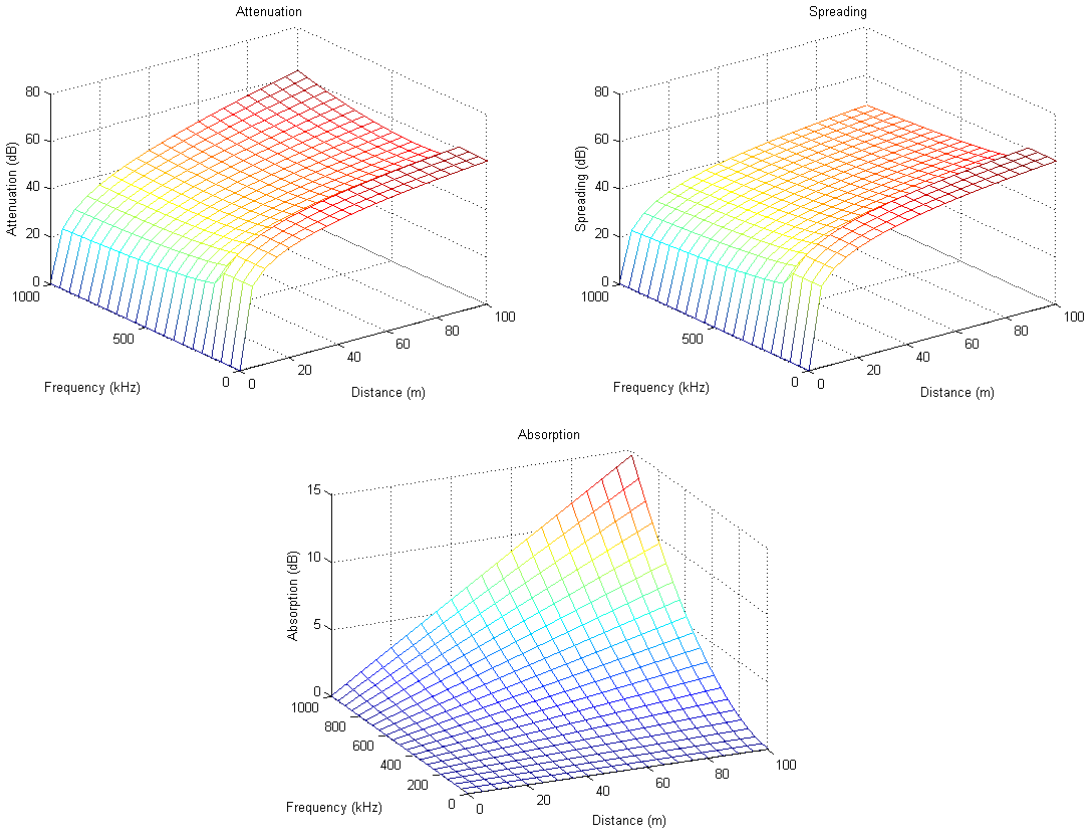

This value also maximizes the available channel bandwidth for communication. For this reason, in the MatLab/Simulink simulations the projector model operates at $1MHz$, with the sampling frequency picked being $25MHz$. The table 5.1 shows the aquarium dimensions and other relevant parameters used for the simulations. In all the simulations figures, the amplitudes are in μPa.

Table 5.1: Other parameters used in simulations

Quantity	Value	Quantity	Value
Piezo sound speed	2250	Transmitter	(23 22,5 11)
Piezo density	1470	Receiver	(23 87,5 15)
Thickness	$28x10^{-6}$	Channel size	(48 120 30)
d33	$34x10^{-12}$	Transducer Radius (cm)	1
Number of layers	8	Shipping factor	1
Gain of the signal	10^6	Wind speed	10
Transducer radius (cm)	10	Doppler	0
Temperature	30	Piezo sound speed	2250
Salinity	1	Piezo density	1470
Acidity of water	7,2	Signal amplitudes	1; 3,5; 9

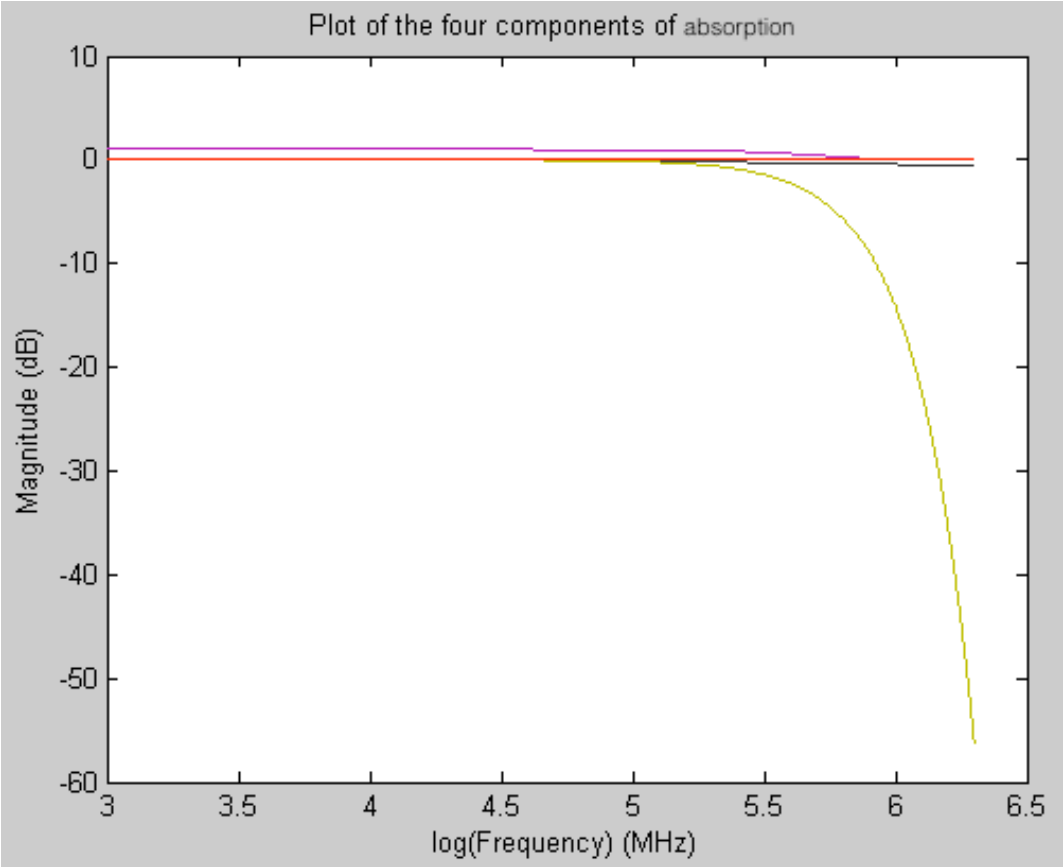

Figure 5.2: Dependence of absorption components with frequency

5.2.1 OOK modulation

For the first simulation, an OOK modulation was considered and the aquarium scenario with the multipath effect was selected. Figures 5.4 and 5.5 show the transmission of an OOK burst of 8bits (alternate one and zero logical levels), repeated each $60\mu s$, with the carrier frequency being $1MHz$. This is done for other modulations with a total of $80\mu s$ of simulation time and the burst during $20\mu s$ of those 60 stated, being 40 of no signal modulation to guard a time for the appearance of multipath contributions.

For this particular case, as can be seen in figure 5.5, the channel output shows the presence of replicas of the input signal due to reflections on the walls and surface that lead to the observed inter-symbol interference (ISI). This case study clearly shows that there are situations where a more robust modulation, regarding the multipath phenomenon, like OFDM, may have to be considered.

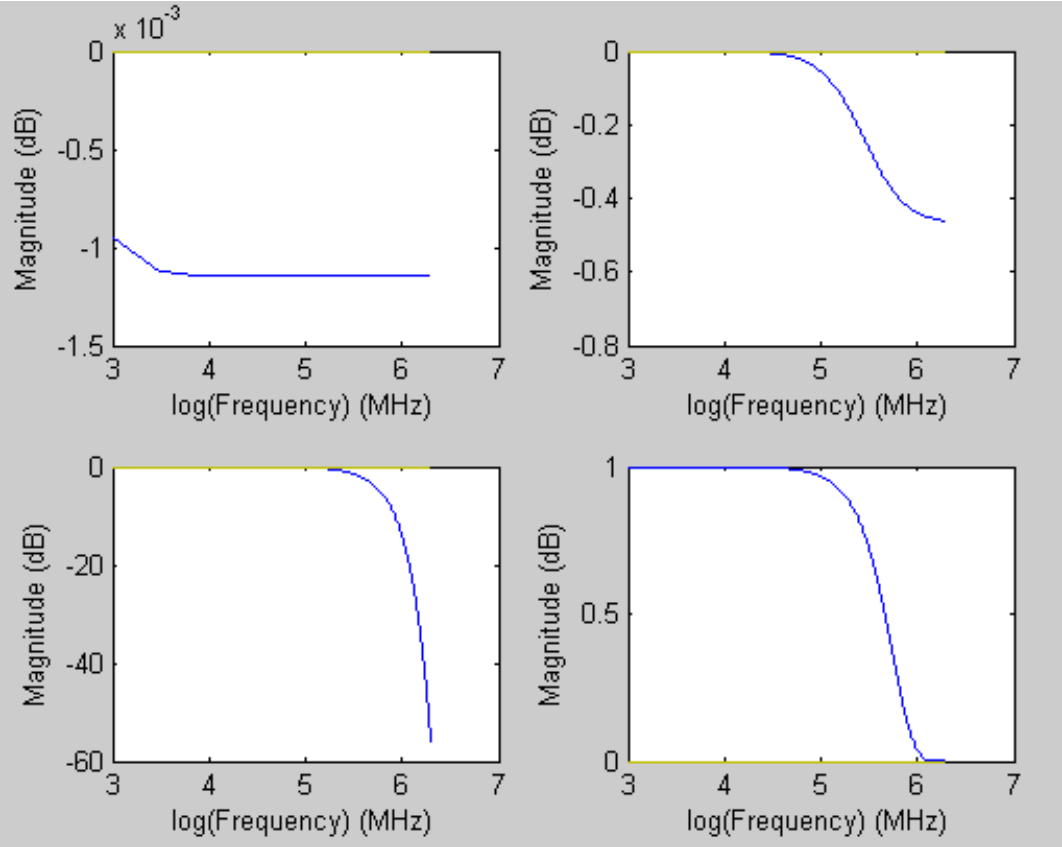

Figure 5.3: Individual plots of the four components of absorption

5.2.2 BASK modulation

In the second example simulated a BASK modulation was used. Figure 5.6 shows this scenario for a burst of alternate logical binary levels. In this case, no multipath effect was inserted into the model.

The corresponding channel output, shown in figure 5.7, reveals the channel bandwidth limitation due to the its low-pass behavior. Notice that the channel response to each logical level lasts more then the bit duration, thus producing inter-symbol interference. This problem leads to a smaller noise margin in the eyepattern and a BER degradation. Furthermore, BASK spends more energy then OOK to reach the same BER performance.

5.2.3 BPSK modulation

For the third case, shown in figure 5.8, the modulation used was changed to BPSK and the multipath module was present again, as was in the case of OOK previously analyzed. The output observed in figure 5.9 reveals the same problem of ISI already seen in the OOK case. Therefore, from this point of view there is no advantage in changing to BPSK, particularly if one takes into account its more difficult demodulation,

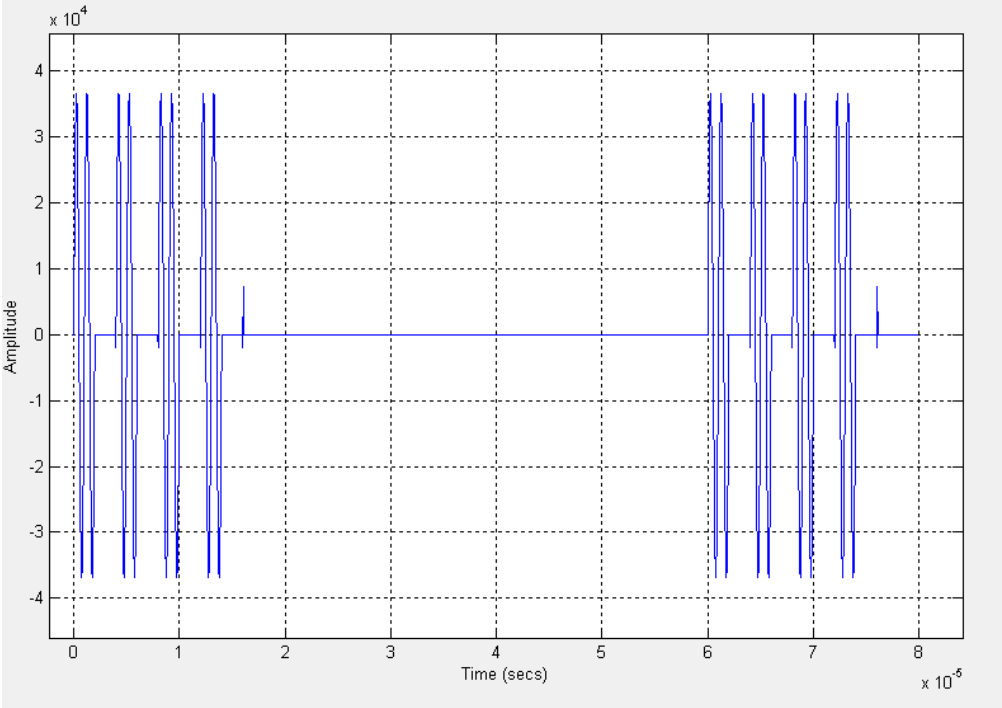

Figure 5.4: OOK signal at the channel input

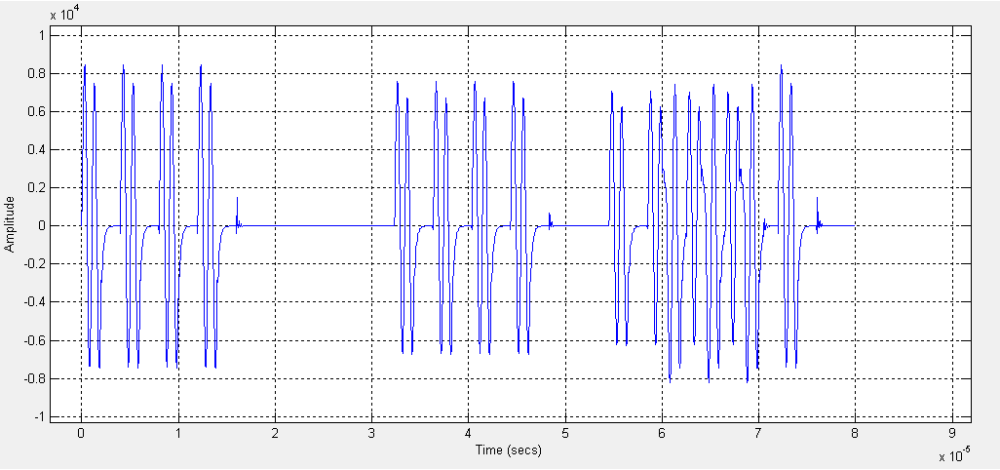

Figure 5.5: OOK signal at the channel output

requiring a more complex (coherent) receiver system. However, if ISI is not present we know from literature and from the revision presented in 2 that BPSK has better BER performance when compared to OOK. This is because, when comparing the two modulations, the constellation points have a greater separation, in the BPSK case. Also a factor, OOK may be much more easily demodulated, using only a simple envelope detector and a comparator which means that a very simple and inexpensive receiver can be used. These are some of the trade-off aspects that have to be considered, when going into a real implementation.

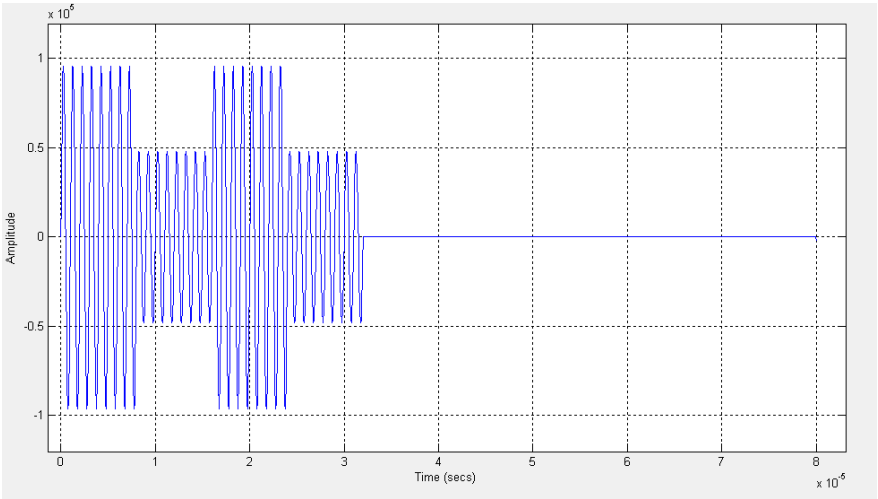

Figure 5.6: BASK signal at the channel input

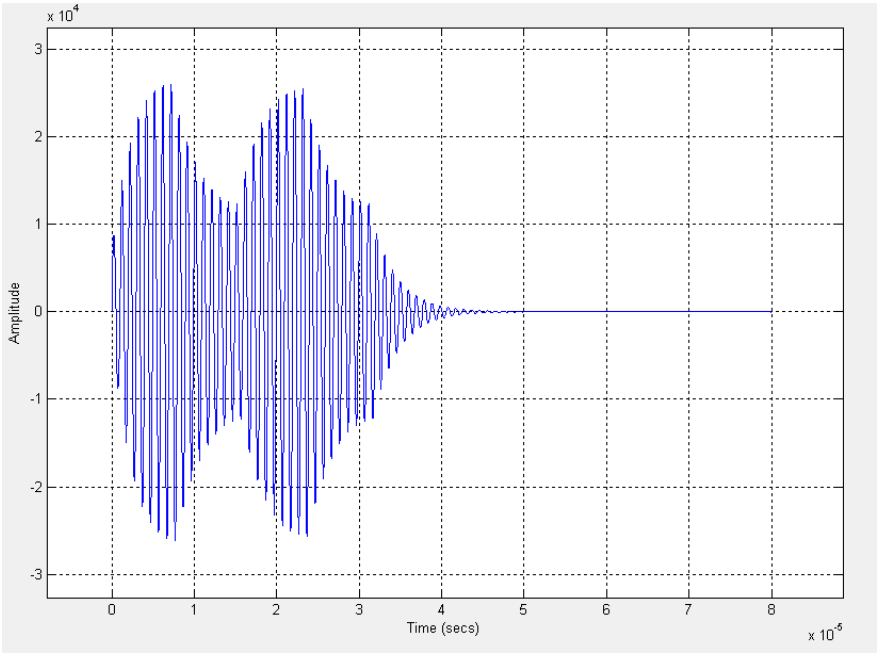

Figure 5.7: BASK signal at the channel input

5.2.4 BFSK modulation

Finally a fourth situation was considered, depicted in figures 5.10 and 5.11, where the modulation used was BFSK and the multipath module was enabled.

To be noticed that the projector model was optimized for an operating frequency of $1MHz$ and it has a bandpass behavior. Different amplitude levels are seen for the two frequencies used. This is not the normal situation for the BFSK signal and should be avoided, as it degrades the BER performance. This happens because the two BPSK constellation points get closer, when different bit energies are used.

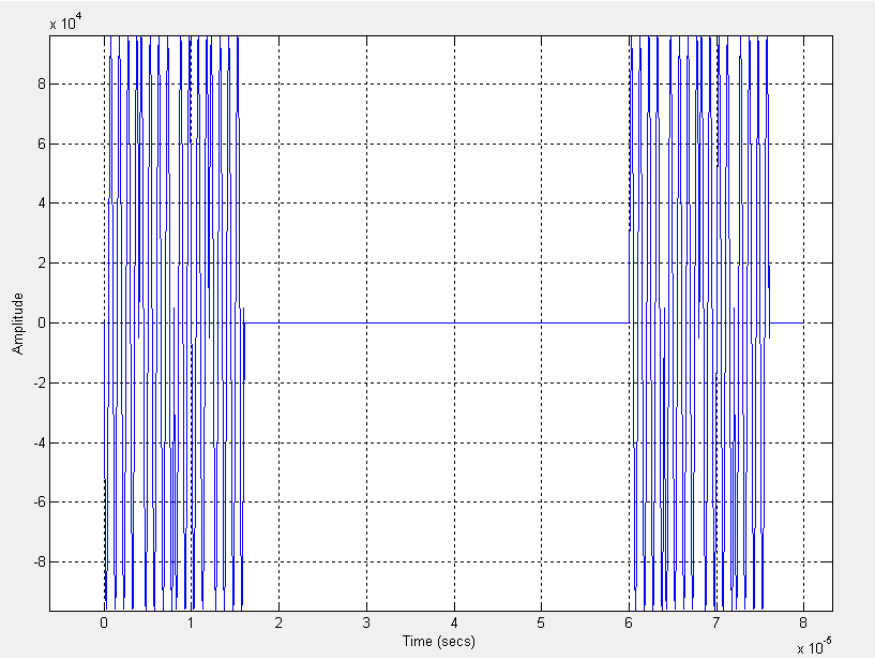

Figure 5.8: BPSK signal at the channel inpu

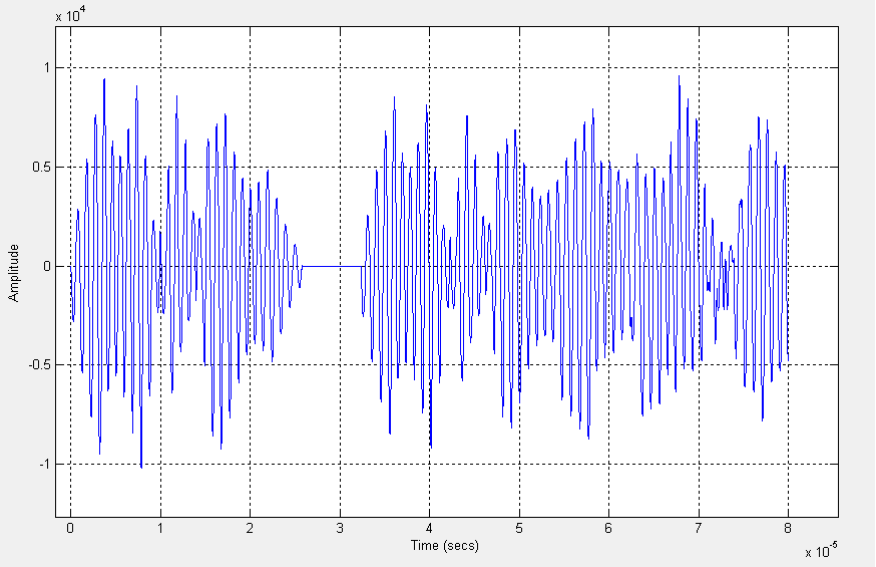

Figure 5.9: BPSK signal at the channel inpu

In this simulation, multipath problems are also present as in the other two cases (OOK and BPSK) so BFSK, as expected, also has no advantages with respect to this multipath ISI situation. For the case when the multipath is absent, one can have a simpler receiver for BFSK (non-coherent) with better BER than for a non-coherent OOK receiver [24].

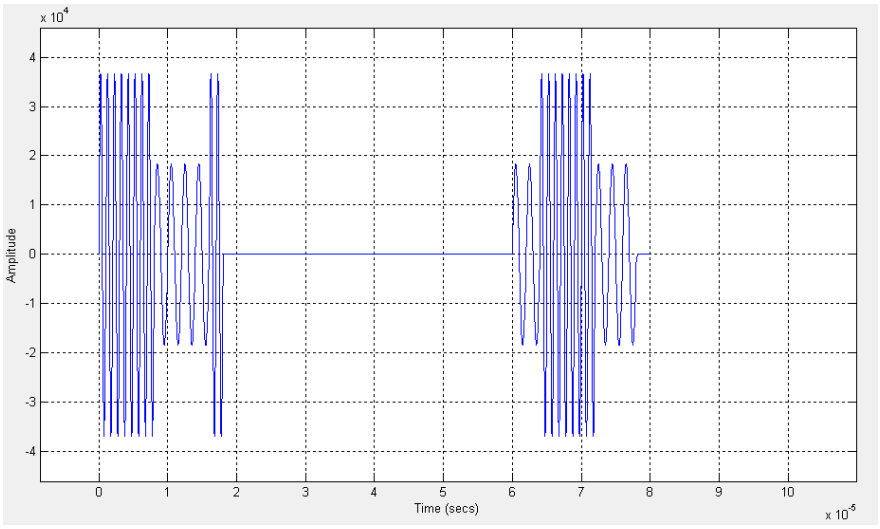

Figure 5.10: BFSK signal at the channel input

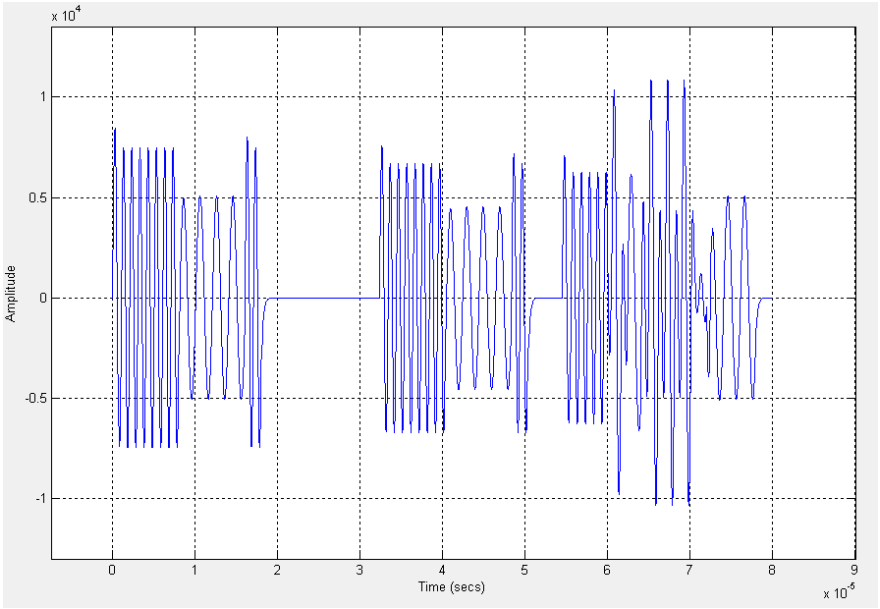

Figure 5.11: BFSK signal at the channel output

5.3 Chapter conclusions

Several modulations were considered and applied to the channel model developed. All show that the multipath effect, when present, may lead to serious difficulties. In situations where the multipath can be neglected, all modulations considered may be used. In such cases, some kind of trade-off, between system complexity and the required BER for the application, must be considered. This may lead to simpler or more complex system implementations, particularly at the receiver end. Finally, some ISI problems were observed in the simulations and this is a situation that needs to be considered and it should degrade the eye

pattern, the noise margin and, consequently, the BER to an unacceptable level.

Chapter 6

Conclusions and Future Work

In this chapter all the work developed during this thesis is briefly presented with emphasis on the results already obtained and future developments, that may lead to improvements for the project.

6.1 Results achieved

The main goal of this work was achieved, creating a channel model that, besides other aspects, contains a multipath block that enables the prediction of these effects in a real environment. A simplified approach to the channel model, by considering different blocks each associated to a particular effect of the underwater channel, was a good solution to start investigations in such a complex field of study, such as underwater acoustic communications.

Using simple sinusoidal signals and modulated tones it was possible at the *Universidade do Minho* to verify in practice the effects of the channel, such as its attenuation, its bandwidth limitations and the presence of delayed replicas of the original signal, which may imply distortion on the received signal. All these effects were considered in the channel model implemented and simulated, so as to obtain the signal at the channel output. Results cannot yet be correlated with the real measurements since the hydrophone MaltLab model is still in the development stage.

Other extra tasks were performed, in order to complement the project with helpful simulation tools, making it possible to define and establish different simulation scenarios. In particular, the preliminary applications developed for MatLab/Simulink will enable to easily simulate proposed cases in which it will be possible to choose the dimensions of the aquatic channel (where the communication takes place) and the type of modulations or techniques applied to the signal.

Given the time scope for the present work, the fact that the area in consideration was completely new and involved hard work to understand its basic fundamentals, we consider that the work done was very satisfactory. It became clear that there are areas where further developments must be done. This will be detailed in the next section, which covers the topic.

6.2 Future developments

The channel simulation model seems to be rather stable and includes all the effects that should be considered relevant. However, it is necessary to be able to compare the simulation results with real world measurements, which can only be done when the hydrophone model is finished.

Another relevant area that requires further study too is the modulation techniques used, where more simulation and testing of various types of modulations need to be done and compared. This may be particularly difficult in scenarios where multipath occurs and so more robust and complex modulation techniques, like OFDM, should be tried. These aspects have to be balanced with coding strategies that can, in some cases, be sufficient to achieve an adequate BER with a simpler modulation. These considerations will largely depend on the application being investigated and the channel characteristics, leading to more complex or simpler solutions.

Finally, compression techniques may also be necessary, in order to reduce the information rate to a desired level, in accordance with the available channel bandwidth, which we know is rather limited in acoustic underwater communications.

It is expected that all this work will lead to a robust underwater communication system that can be used for example in rivers with ranges from 50 to 100m.

Appendix A

Schematics and schemes

A.1 Schematic of the complete underwater system

The following schematic is the MatLab/Simulink model developed for the underwater acoustic communication system. Notice the presence of a block that models the projector and the absence of the hydrophone model block, being developed.

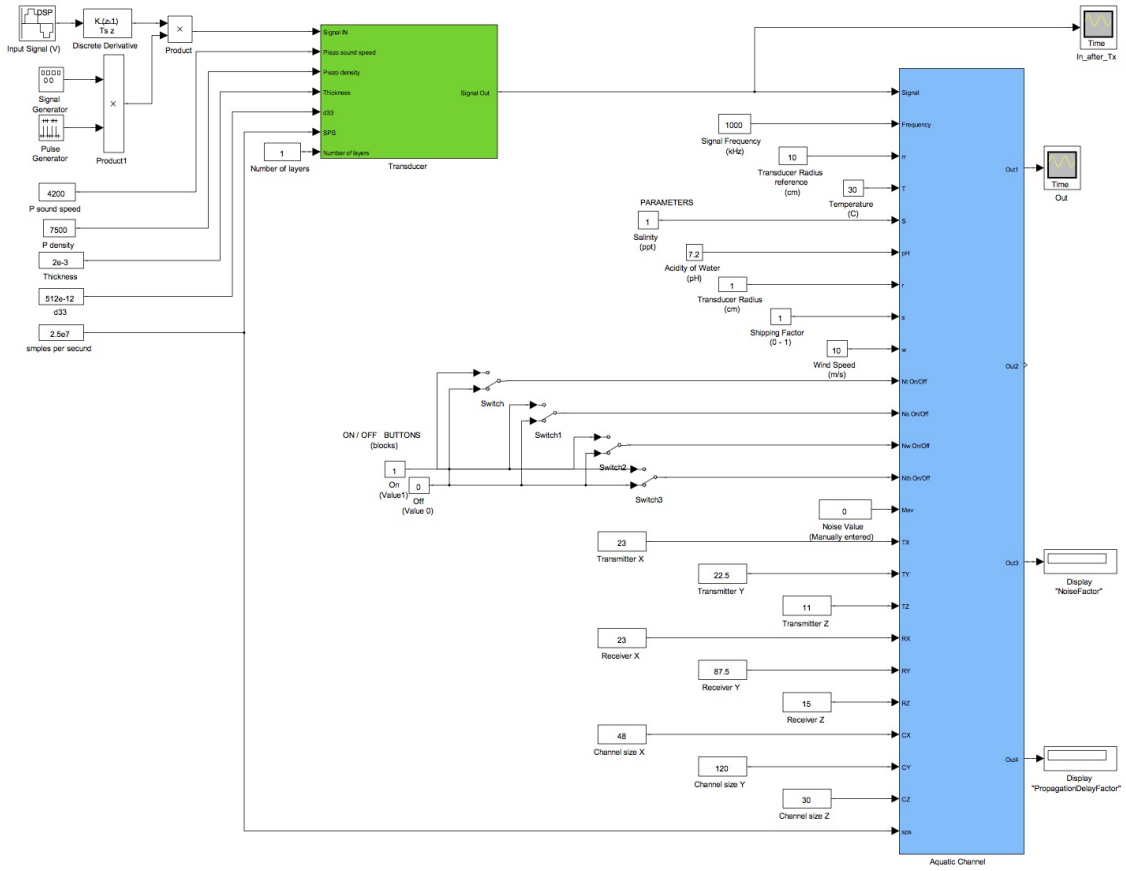

Figure A.1: Underwater communication system model

A.2 Schematic of the aquatic channel

Schematic showing the developed aquatic channel model with all the blocks considered, including the multipath block. The MatLab codes are presented in annex B

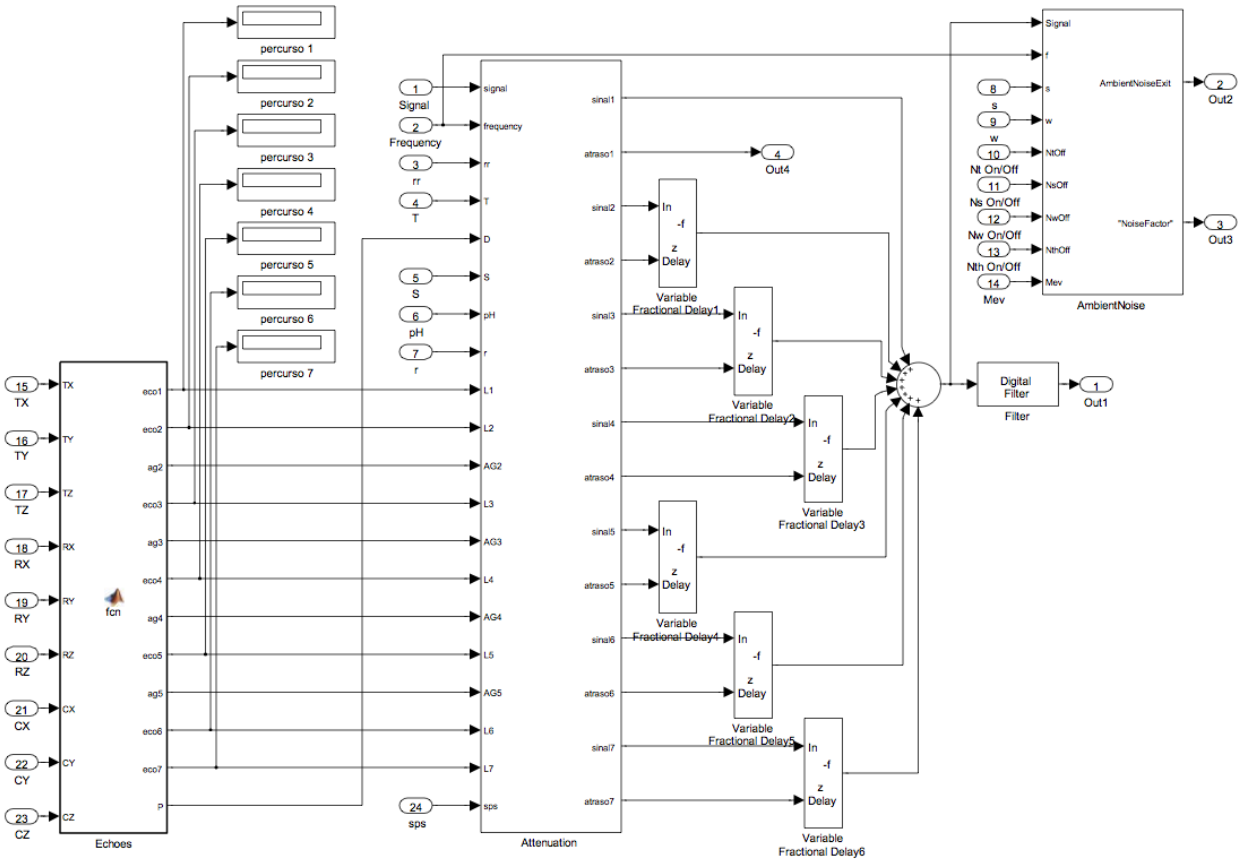

Figure A.2: Module of aquatic channel

A.3 Aquarium multipath schemes

As a first case we consider the simplest multipath geometry in which the projector and the hydrophone are aligned with the same x and z coordinates and centered at the vertical tops of the aquarium. The four minimum reflection paths are in two pairs due to width and height being different. Only if these two dimensions were the same the four paths would be equal.

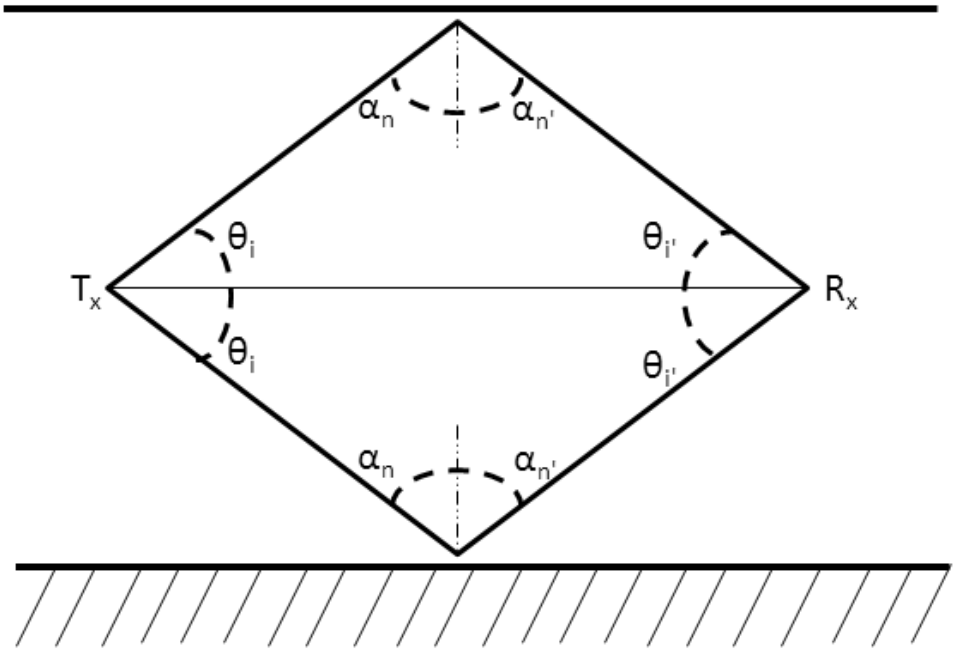

Figure A.3: First case of reflection

In the second one we see the particular case in which the projector and the hydrophone are misaligned with the same x and different z coordinates (could be the inverse being the same z and different x) at the vertical tops of the aquarium. But there is some other particularity that is the distance of the projector to the surface is equal to the distance of the hydrophone to the bottom making again four minimum paths in pairs.

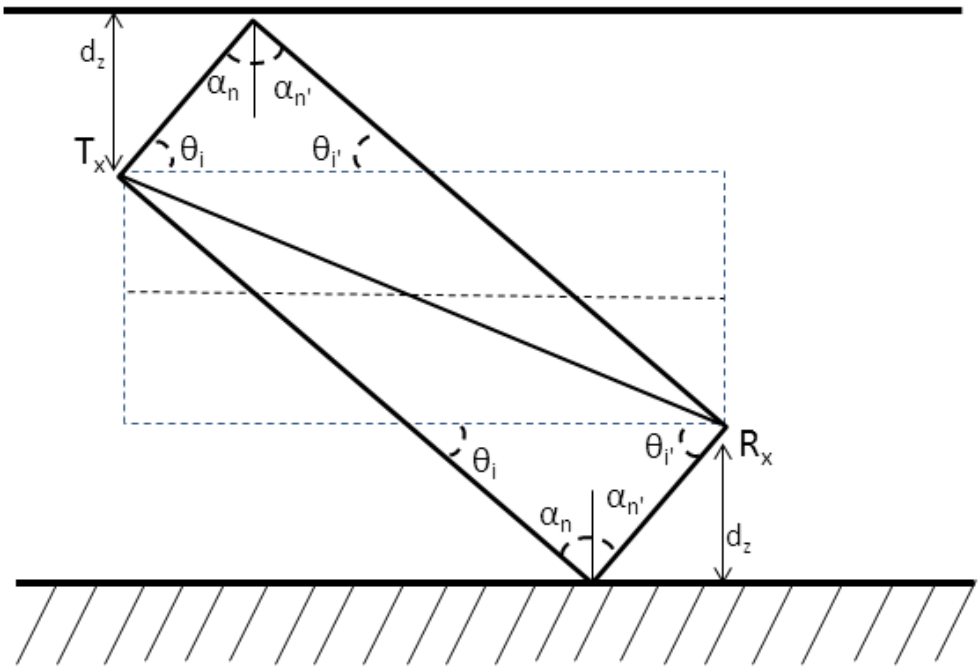

Figure A.4: Second case of reflection

This is the general case with misalignment of transmitter and the receiver devices. Note the distance of projector is different to the top from the hydrophone to the bottom. The angles are even more different than the other case noting still there are equal angle pairs.

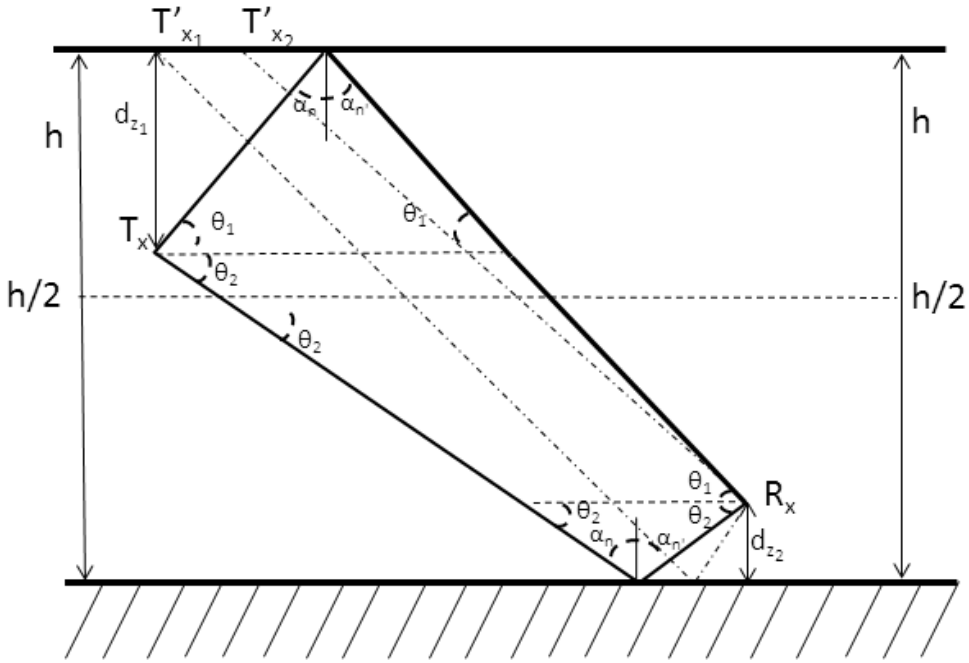

Figure A.5: Third case of reflection

Appendix B

MatLab blocks and modules code

Every schematics and code are present in this Appendix

B.1 Attenuation code

The written code to implement the attenuation effect is shown below.

```
%-----------------------------------------------------------
% Written by Julio Xavier/Feb2011 using some structure code of previous
% code from the project developments
% MatLab/Simulink simulation code from blocks of Simulink for Master Thesis
% Title - "Modulation Analysis for an Underwater Communication Channel"
% Mestrado Integrado em Engenharia Electrot\'ecnica e de Computadores
% Master of Science in Electrical and Computer Engineering
% Faculdade de Engenharia da Universidade do Porto
% Faculty of Engineering - University of Porto

%Bloc attenuation
%Function Definition
function [sg1,at1,sg2,at2,sg3,at3,sg4,at4,sg5,at5,sg6,at6,sg7,at7, agT]
 = fcn(f,L1,L2,ag2,L3,ag3,L4,ag4,L5,ag5,L6,L7, T,D, S, pH, rr, r, sps)

%Parameter Values (Boric Acid and Magnesium Sulphate)
f1 = 0.78 * sqrt(S/35) * (exp(T/26));
f2 = 42 * (exp(T/17));

%Speed of sound (m/s)
cmetro = 1448.96 + 4.591*T - 5.304*(10^(-2))*(T^(2)) +
 + 2.374*(10^(-4))*(T^(3))
 + 1.340*(S-35) + 1.630*(10^(-2))*D + 1.675*(10^(-7))*(D^(2)) +
  - 1.025*(10^(-2))*T*(S-35) - 7.139*(10^(-13))*T*(D^(3));
```

```
%Conversion from m/s to cm/s
c=cmetro*100;

%Calculation of wavelength
lambda = c/(f*1000);

%Calculation of the transducer diameter
angulo=0;
d = 2*r;
de=(pi*rr^2);

%Absorption Coefficient
a = ((0.106 * (f1 * f^2) * exp((pH - 8)/0.56)) / (f1^2 + f^2)) +
 + ((0.52 * (1 + (T/43)) * (S/45) * (f2 * f^2) *
 * exp(-(D/6))) / (f2^2 + f^2)) + (0.00049 * (f^2) * (exp(-(T/27 + D/17))));

%Attenuation
ab1 = a*(L1/1e5);

ab2 = a*(L2/1e5);

ab3 = a*(L3/1e5);

ab4 = a*(L4/1e5);

ab5 = a*(L5/1e5);

ab6 = a*(L6/1e5);

ab7 = a*(L7/1e5);

if r < lambda;
   angulo = pi/2;
end
if r > lambda;
   angulo = asin(lambda/d);
end

sp1 = 10*log10(((2*angulo*(L1)^2) + de)/de);
sp2 = 10*log10(((2*angulo*(L2)^2) + de)/de);
sp3 = 10*log10(((2*angulo*(L3)^2) + de)/de);
sp4 = 10*log10(((2*angulo*(L4)^2) + de)/de);
sp5 = 10*log10(((2*angulo*(L5)^2) + de)/de);
```

```
sp6 = 10*log10(((2*angulo*(L6)^2) + de)/de);
sp7 = 10*log10(((2*angulo*(L7)^2) + de)/de);

sg1 = 0;
sg2 = 0;
sg3 = 0;
sg4 = 0;
sg5 = 0;
sg6 = 0;
sg7 = 0;

at1=0;
at2=0;
at3=0;
at4=0;
at5=0;
at6=0;
at7=0;

    sg1= 10^((-1*(ab1 + sp1))/10);
    at1= ((L1/c)*sps);

%if(ag2<=angulo)
    sg2 = 10^((-1*(ab2 + sp2))/10);
    at2= ((L2/c)*sps)-at1;
%end
%if(ag3<=angulo)
    sg3 = 10^((-1*(ab3 + sp3))/10);
    at3= ((L3/c)*sps)-at1;
%end
%if(ag4<=angulo)
    sg4 = 10^((-1*(ab4 + sp4))/10);
    at4= ((L4/c)*sps)-at1;
%end
%if(ag5<=angulo)
    sg5 = 10^((-1*(ab5 + sp5))/10);
    at5= ((L5/c)*sps)-at1;
%end

if (L6>0)
    sg6 = 10^((-1*(ab6 + sp6))/10);
    at6= ((L6/c)*sps)-at1;
end
if (L7>0)
```

```
    sg7 = 10^((-1*(ab7 + sp7))/10);
    at7= ((L7/c)*sps)-at1;
end

at1=at1/sps;
agT=angulo;
```

B.2 Multipath code

The written code to implement the multipath effect is shown below.

```
%Bloc echoes
%Function Definition
function [eco1,eco2,ag2,eco3,ag3,eco4,ag4,eco5,ag5,eco6,eco7,P]
 = fcn(TX,TY,TZ,RX,RY,RZ,CX,CY,CZ)


%   D1=sqrt( (x2-x1)^2 + (y2-y1)^2 + (z2-z1)^2 )
%
%
%%  Rxc2 = [2*w-x2, y2, z2]
%
%       D2=sqrt( ((2*w-x2)-x1)^2 + (y2-y1)^2 + (z2-z1)^2 )
%
%
%%  Rxc3 = [-x2, y2, z2]
%
%       D3=sqrt( (-x2-x1)^2 + (y2-y1)^2 + (z2-z1)^2 )
%
%
%%  Rxc4 = [x2, y2, 2*D-z2]
%
%       D4=sqrt( (x2-x1)^2 + (y2-y1)^2 + ((2*D-z2)-z1)^2 )
%
%
%%  Rxc5 = [x2, y2, -z2]
%
%       D5=sqrt( (x2-x1)^2 + (y2-y1)^2 + (-z2-z1)^2 )
%
% Case z1==z2, i.e. at the same level the echoes are the same
%
%%  Rxc6 = [x2, -y2, z2]
%
%       D4=sqrt( (x2-x1)^2 + (-y2-y1)^2 + (z2-z1)^2 )
%
%
%%  Rxc7 = [x2, 2*L-y2, z2]
%
%       D5=sqrt( (x2-x1)^2 + ((2*L-y2)-y1)^2 + (z2-z1)^2 )
%
%result signal
```

```
eco1 = sqrt((RX-TX)^2 + (RY-TY)^2 + (RZ-TZ)^2);

eco2 = sqrt( ((2*CX-RX)-TX)^2 + (RY-TY)^2 + (RZ-TZ)^2 );

ag2 = asin(abs((2*CX-RX)-TX)/eco2);

eco3 = sqrt( (-RX-TX)^2 + (RY-TY)^2 + (RZ-TZ)^2 );

ag3 = asin((RX+TX)/eco3);

eco4 = sqrt( (RX-TX)^2 + (RY-TY)^2 + ((2*CZ-RZ)-TZ)^2 );

ag4 = asin(abs((2*CZ-RZ)-TZ)/eco4);

eco5 = sqrt( (RX-TX)^2 + (RY-TY)^2 + (-RZ-TZ)^2 );

ag5 = asin((RZ+TZ)/eco5);

if((RZ==TZ) && (RX==TX))
   eco6 = (RY+TY);

   eco7 = sqrt(((2*CY-RY)-TY)^2);
else
   eco6 = 0;

   eco7 = 0;
end

P=(RZ+TZ)/2;
```

B.3 Filter code

The written code to implement the filter is shown below.

```
function Hd = filter_FIR
% All frequency values are in MHz.
Fs = 25;  % Sampling Frequency

N    = 10;       % Order
Fc   = 2;        % Cutoff Frequency
flag = 'scale';  % Sampling Flag

% Create the window vector for the design algorithm.
win = rectwin(N+1);

% Calculate the coefficients using the FIR1 function.
b  = fir1(N, Fc/(Fs/2), 'low', win, flag);
Hd = dfilt.dffir(b);

% [EOF]
```

B.4 Ambient noise code

The written code to implement the ambient noise effect is shown below.

```
%Ambient noise block
%Function Definition
function saida = fcn(f, s, w, NtOff, NsOff, NwOff, NthOff, Mev)

% f - signal frequency (kHz); s - shipping factor (between 0 - 1);
% w - wind speed (m/s); NtOff, NsOff, NwOff, NthOff - Disable the
% corresponding equation;
% Mev - Manually entered value.


%Equation of Turbulence Noise
Nt = (10^((17-30*log10(f))/10))*NtOff;

%Equation of Shipping Noise
Ns = (10^((40+(20*(s-0.5))+(26*log10(f))-(60*log10(f+0.03)))/10))*NsOff;

%Equation of Wave Noise
Nw = (10^((50+(7.5*(w^(1/2)))+(20*log10(f))-(40*log10(f+0.4)))/10))*NwOff;

%Equation of Thermal Noise
Nth = (10^((-15+20*log10(f))/10))*NthOff;

%Total Noise
saida = Nt + Ns + Nw + Nth + Mev;
```

B.5 Signal with added noise code

```
%Signal noisy block
%Function Definition
function saida = fcn(sinal, value)

saida=sinal;
   r1 = randn(1)/12;
   r2 = randn(1)/6.8;
   r3 = randn(1)/136;
   r4 = randn(1)/3;
   r5 = randn(1)/56;
   r6 = randn(1)/7.9;
   r7 = randn(1)/2.5;
   r8 = randn(1)/0.1;
   r9 = randn(1)/1.1;
   r10 = randn(1)/0.29;
   r11 = r10*1.15;
for i = 1:numel(sinal)
  saida(i) = sinal(i)+ 0.7*value*(sin(r1*i)+ sin(r2*i)+ sin(r3*i)+ sin(r6*i)+
 + sin(r4*i) +  sin(r5*i) + sin(r7*i)+ sin(r8*i)+ sin(r9*i)+ sin(r10*i)+
 + sin(r11*i) + 3*randn(1));
end
```

B.6 Attenuation profiles

The written code to implement the attenuation profiles plots is shown below.

```
%-------------------------------------------------------------------------
%  Parameter values that influences the attenuation of underwater mean
%-------------------------------------------------------------------------

T = 32;         % Temperature (C)
S = 1;          % Salinity (ppt)
D = 1;          % Depth (m)
pH = 7.2;       % pH
f1 = 0.78 * sqrt(S/35) * (exp(T/26));          % Boric acid
f2 = 42 * (exp(T/17));         % Magnesium sulfate

%-------------------------------------------------------------------------
%  Auxiliary variables
%-------------------------------------------------------------------------

r = 1;          % Transducer radium (cm)
rr = 10;        % Reference radium
step = 500;          % Jump between distances in (cm)
l = 0:step:(step*20+r);       % Emitter to receiver distance
f = 0:50:1001;      % Signal frequency (kHz)

% Transducer diameter calcule
d = 2*r;
f(1)=1;
l(1)=r;
%-------------------------------------------------------------------------
% Samples number for the graph
%-------------------------------------------------------------------------

saida = zeros(21,21);
saida2 = zeros(21,21);
saidat = zeros(21,21);
a = zeros(21);
lambda = zeros(21);
angulo = zeros(21);
de = zeros(21,21);
nm= zeros(21,21);
%-------------------------------------------------------------------------
%  Sound speed calculus on water (m/s)
%-------------------------------------------------------------------------
```

```
cmetro = 1448.96 + 4.591*T - 5.304*(10^(-2))*(T^(2)) + 2.374*(10^(-4))*...
(T^(3)) + 1.340*(S-35) + 1.630*(10^(-2))*D + 1.675*(10^(-7))*(D^(2)) -...
1.025*(10^(-2))*T*(S-35) - 7.139*(10^(-13))*T*(D^(3));

% disp('Sound speed (m/s):');
%disp(c);
c=cmetro*100;

%------------------------------------------------------------------------
%  Cycle for the calculus of Coefficient of Absorption and attenuation
%------------------------------------------------------------------------

for i = 1:1:21;
    % Counter that represents the distance (to simulate the behavior of
    % attenuation through several distances)

    for j = 1:1:21;
        % Counter that represents the frequency (to simulate the behavior of
        % attenuation through several frequencies)


      % Wavelength calculus
      lambda(j) = c/(f(j)*1000);
      %disp('wavelength');
      %disp(lambda);

      % Absorption coefficient
      a(j) = (((0.106 * (f1 * f(j)^2) * exp((pH - 8)/0.56)) / (f1^2 +...
          f(j)^2)) + ((0.52 * (1 + (T/43)) * (S/45) * (f2 * f(j)^2) *...
          exp(-(D/6))) / (f2^2 + f(j)^2)) + (0.00049 * (f(j)^2) *...
          (exp(-(T/27 + D/17)))));

      % Attenuation (dB)
      %saida(j,i) = -10*log(((2*(angulo)*(l(i))^2)/(pi*r^2))+a(j));
      saida(j,i) = a(j)*((l(i))/1e5);

      de=(pi*rr^2);
      %angulo(j) = asin(lambda(j)/d);
      if r<lambda(j);
          angulo(j) = pi/2;
          nm(j,i)=(2*angulo(j)*(l(i))^2);
      end
      if r>=lambda(j);
          angulo(j) = asin(lambda(j)/d);
```

```
            nm(j,i)=(2*angulo(j)*(l(i))^2);
        end
         saida2(j,i)=10*log10(nm(j,i)/de + 1);
    saidat(j,i)=saida(j,i)+saida2(j,i);
    end
end

%-------------------------------------------------------------------------
%  Graphs
%-------------------------------------------------------------------------

saida(1,1)=0;
saida2(1,1)=saida2(2,1);
%subplot(2,1,1);
figure(1);
mesh((l-r)/100,f,saida);
title('Absorption');
shading interp;
xlabel('Distance (m)');
ylabel('Frequency (kHz)');
zlabel('Absorption (dB)');

%subplot(2,1,2)
figure(2);
mesh((l-r)/100,f,saida2, 'EdgeColor','none');
title('Spreading');
shading interp;
xlabel('Distance (m)');
ylabel('Frequency (kHz)');
zlabel('Spreading (dB)');

figure(3);
mesh((l-r)/100,f,saidat, 'EdgeColor','none');
title('Attenuation');
shading interp;
xlabel('Distance (m)');
ylabel('Frequency (kHz)');
zlabel('Attenuation (dB)');
```

B.7 Attenuation function

The written code to implement the attenuation function plots is shown below.

```
%------------------------------------------------------------------------
%  Parameter values that influences the attenuation of underwater mean
%------------------------------------------------------------------------

T = 32;                                                 % Temperature (C)
S = 1;                                                  % Salinity (ppt)
D = 1;                                                % Depth (m)
pH = 7.2;                                               % pH
f1 = 0.78 * sqrt(S/35) * (exp(T/26));     % Boric acid
f2 = 42 * (exp(T/17));                                %Magnesium sulfate
%------------------------------------------------------------------------
%  Auxiliary variables
%------------------------------------------------------------------------

f = 1:2:2000;
% Signal frequency(kHz)
% Transducer diameter calculus



%------------------------------------------------------------------------
%  Samples number for the graph
%------------------------------------------------------------------------



a1 = zeros(1000);
a2 = zeros(1000);
a3 = zeros(1000);
a4 = zeros(1000);

%------------------------------------------------------------------------
%  Sound speed calcule on water (m/s)
%------------------------------------------------------------------------

cmetro = 1448.96 + 4.591*T - 5.304*(10^(-2))*(T^(2)) + 2.374 *...
         (10^(-4))*(T^(3)) + 1.340*(S-35) + 1.630*(10^(-2))*D +...
         1.675*(10^(-7))*(D^(2)) - 1.025*(10^(-2))*T*(S-35) -...
         7.139*(10^(-13))*T*(D^(3));
%disp('Sound speed (m/s):'); disp(c);
c=cmetro*100;
%------------------------------------------------------------------------
%  Cycle for the calculate of Coefficient of Absorption and attenuation
```

```
%--------------------------------------------------------------------------

    for j = 1:1:1000;
     % Counter that represents the frequency (to simulate the behavior of
     % attenuation through several frequencies)

      % Absorption coefficient
      a1(j) = (((0.106 * (f1 * f(j)^2) *...
               exp((pH - 8)/0.56)) / (f1^2 + f(j)^2))/-10);
      a2(j) = (((0.52 * (1 + (T/43)) * (S/45) *...
               (f2 * f(j)^2) * exp(-(D/6))) / (f2^2 + f(j)^2))/-10);
      a3(j) = ((0.00049 *(f(j)^2) * (exp(-(T/27 + D/17))))/-10);
    %  a4(j)=a1(j)+a2(j)+a3(j);
    a4(j)= 10^(a3(j)/10);
      % Attenuation (dB)
      %saida(j,i) = -10*log(((2*(angulo)*(l(i))^2)/(pi*r^2))+a(j));

    end


%--------------------------------------------------------------------------
%  Graphics
%--------------------------------------------------------------------------
figure(1);
plot(log10(f*1000),a1);
hold all
plot(log10(f*1000),a2);
hold all
plot(log10(f*1000),a3);
hold all
plot(log10(f*1000),a4);
xlabel('Frequency (MHz)')
ylabel('Magnitude (dB)')
title('Plot of the four components of attenuation')

figure(2)
subplot(2,2,1); plot(log10(f*1000),a1);
xlabel('log(Frequency) (MHz)')
ylabel('Magnitude (dB)')
subplot(2,2,2); plot(log10(f*1000),a2);
xlabel('log(Frequency) (MHz)')
ylabel('Magnitude (dB)')
subplot(2,2,3); plot(log10(f*1000),a3);
xlabel('log(Frequency)(MHz)')
```

```
ylabel('Magnitude (dB)')
subplot(2,2,4); plot(log10(f*1000),a4);
xlabel('log(Frequency) (MHz)')
ylabel('Magnitude (dB)')
title('Subplots of the four components of attenuation')
```

Appendix C

Channel GUI application for MatLab with multipath calculator tool

C.1 GUI figure 1

This first image is the application window which shows the action of button 1, where appears a 2D plane of a monopole emitting acoustic waves in omnidirectional way only limited by the left boundary.

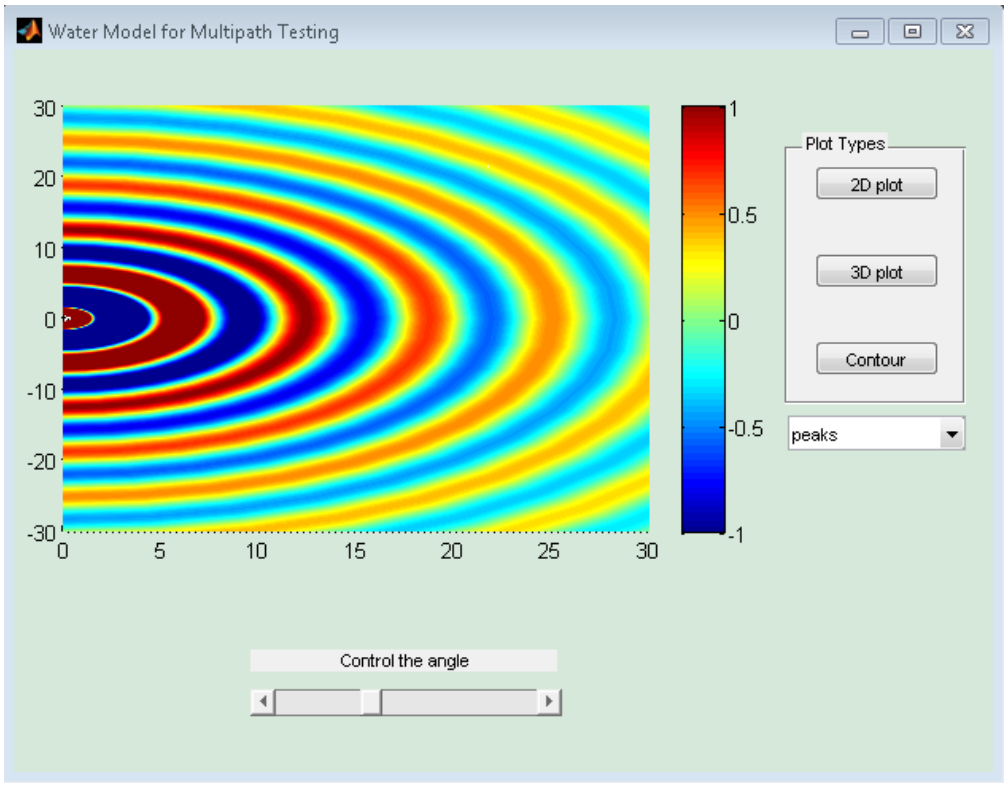

Figure C.1: GUI application: example window 1

C.2 GUI example 2

In this second one is the application window showing the action of button 2 plotting the 3D graph of the monopole source.

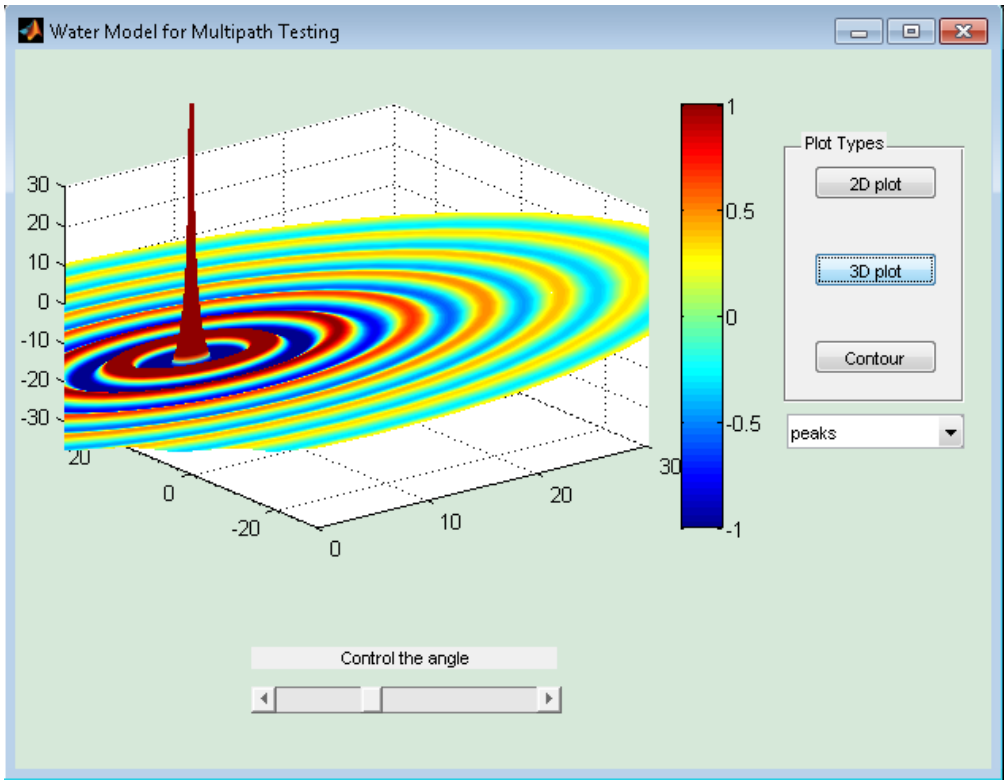

Figure C.2: GUI application: example window 2

C.3 GUI example 3

This third picture is the window plotting of the minimum multipath calculator tool.

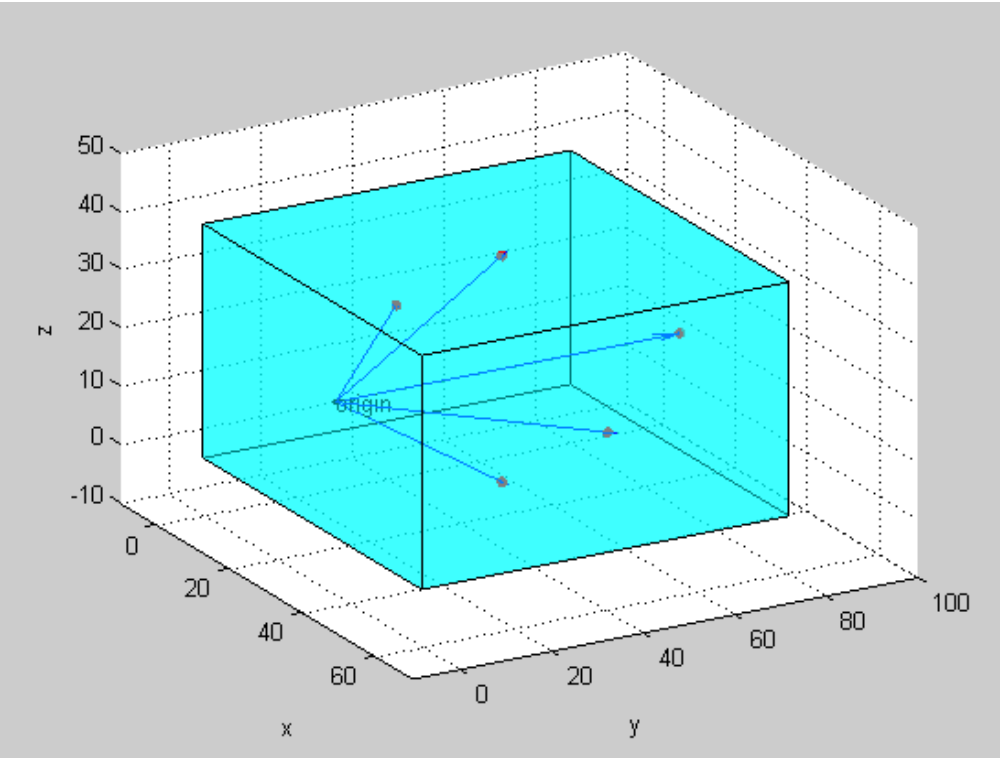

Figure C.3: Minimum multipath calculator tool

C.4 GUI example 4

The last is the development of the route calculator tool inside the MatLab application associated with the third button.

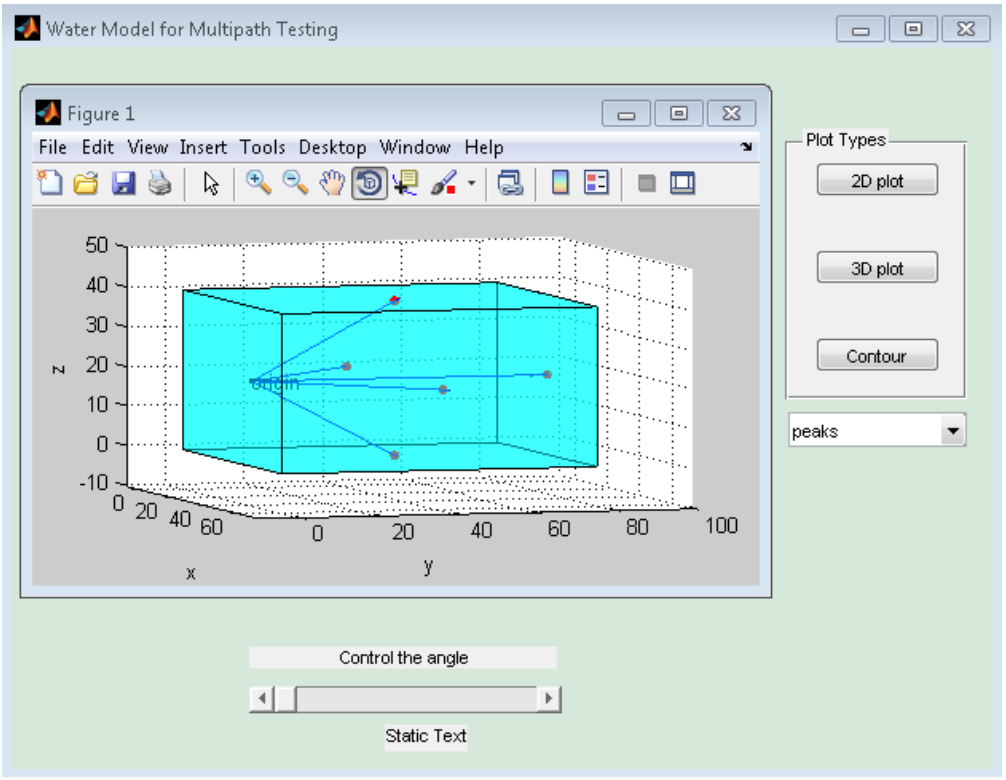

Figure C.4: GUI application: example window 3

Appendix D

Multipath MatLab application

D.1 MatLab example of multipath with Rayleigh channel model

```
Ts = 1e-4;    % Sample period (s)
fd = 100;     % Maximum Doppler shift

% Path delay and gains
tau = [0.1 1.2 2.3 6.2 11.3]*Ts;
PdB = linspace(0, -10, length(tau)) - length(tau)/20;

nTrials = 10000;    % Number of trials
N = 100;            % Number of samples per frame

h = rayleighchan(Ts, fd, tau, PdB);  % Create channel object
h.NormalizePathGains = false;
h.ResetBeforeFiltering = false;
h.StoreHistory = 1;
h % Show channel object

% Channel fading simulation
for trial = 1:nTrials
    x = randint(10000, 1, 4);
    dpskSig = dpskmod(x, 4);
    y = filter(h, dpskSig);
    plot(h);
    % The line below returns control to the command line in case
    % the GUI is closed while this program is still running
    if isempty(findobj('name', 'Multipath Channel')), break; end;
end
```

D.2 MatLab figure application of multipath with Rayleigh channel model with diverse analysis

This window application from MatLab/Simulink implement several analysis of an Rayleigh channel model.

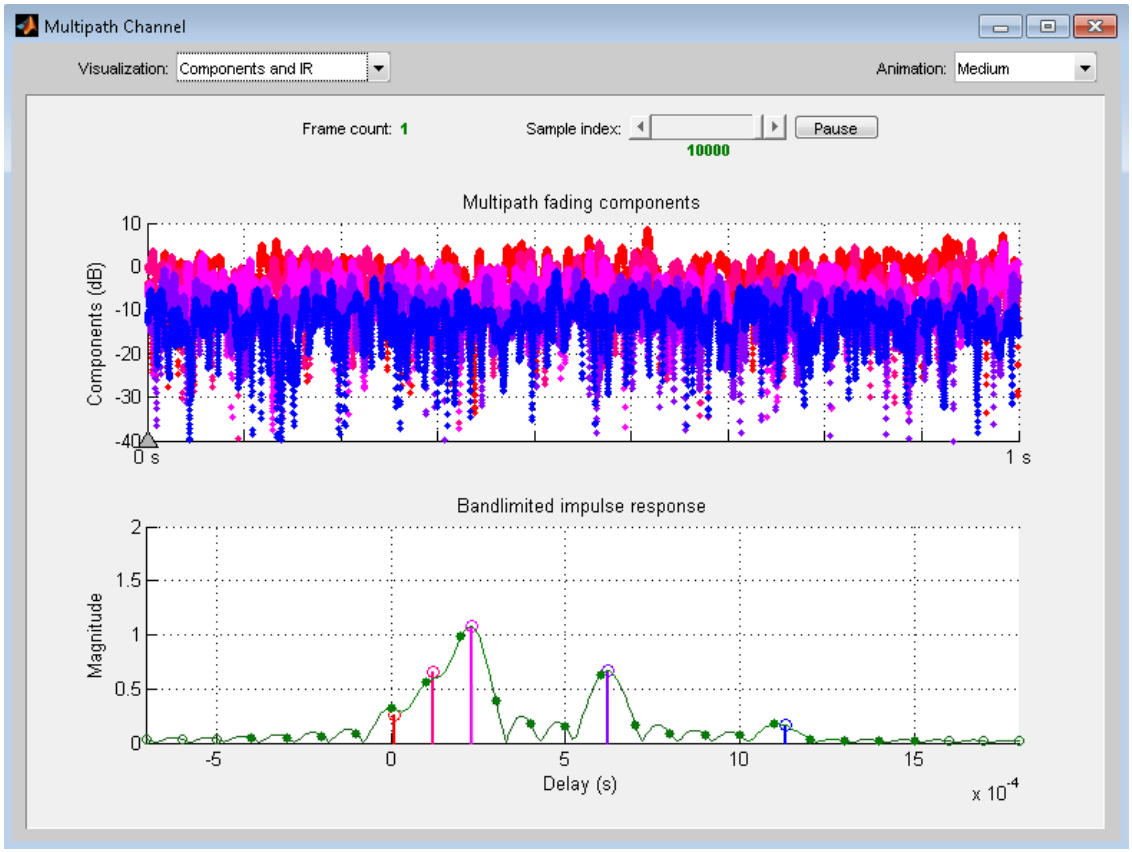

Figure D.1: Multipath channel Graphical User Interface application in MatLab

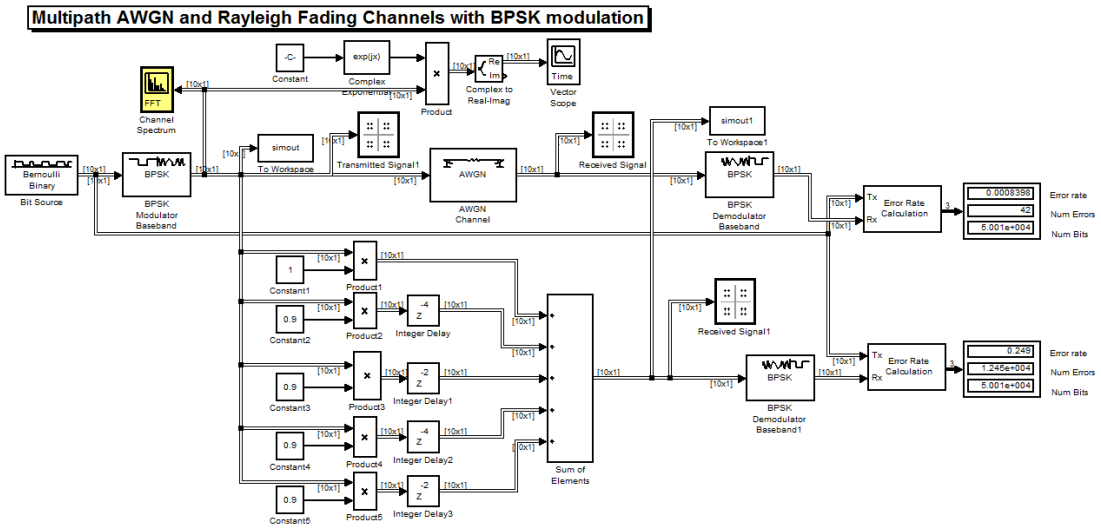

Figure D.2: Simulink model for testing BPSK with a multipath Rayleigh channel

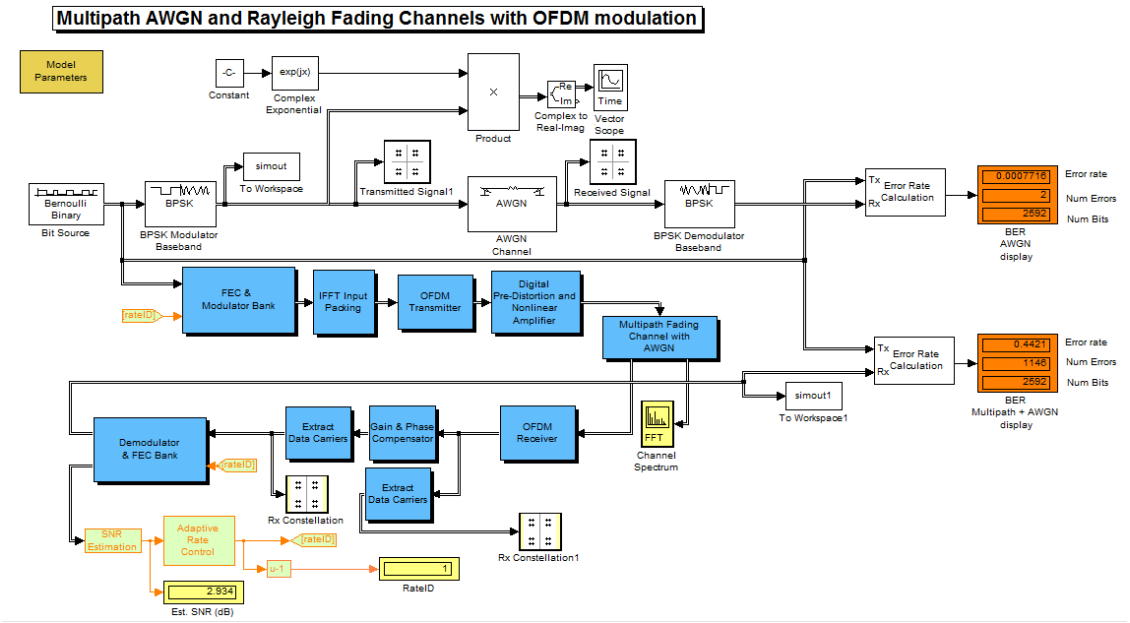

Figure D.3: Simulink model for testing OFDM with a multipath Rayleigh channel

References

[1] Diogo Mendes. A matlab/simulink model to evaluate underwater acoustic. Master's thesis, Universidade do Minho, Portugal, December 2011.

[2] CIA. The world factbook, 2012. Available at https://www.cia.gov/library/publications/the-world-factbook/geos/xx.html#Geo Lastchecked:10 Oct, 2012.

[3] Dosits. Speed of sound, 2012. Available at http://www.dosits.org/science/soundmovement/speedofsound/ Lastchecked: 10 Oct, 2012.

[4] Daniel A. Russell. Radiation from a baffled piston, 2012. Available at http://www.acs.psu.edu/drussell/demos/baffledpiston/baffledpiston.html Lastchecked:10 Oct, 2012.

[5] Kalangi Pullarao Prasanth. Modelling and simulation of an underwater acoustic communication channel. Master's thesis, University of applied sciences Bremen, Germany, 2004.

[6] M. Stojanovic. Recent advances in high-speed underwater acoustic communications. *Oceanic Engineering, IEEE Journal of*, 21(2):125–136, 1996.

[7] Dario Pompili and Ian F. Akyildiz. Overview of networking protocols for underwater wireless communications. *Comm. Mag.*, 47(1):97–102, January 2009.

[8] M. Schroeder, Thomas D. Rossing, F. Dunn, W. M. Hartmann, D. M. Campbell, and N. H. Fletcher. *Springer Handbook of Acoustics*. Springer Publishing Company, Incorporated, 1st edition, 2007.

[9] Gunilla Burrowes and Jamil Y. Khan. Short-range underwater acoustic communication networks. *Autonomous Underwater Vehicles, Mr. Nuno Cruz (Ed.)*, 2011.

[10] A.D. Waite. *Sonar for practising engineers*. Wiley, 2002.

[11] R.J. Urick. *Principles of underwater sound*. McGraw-Hill, 1983.

[12] Mari Carmen Domingo. Overview of channel models for underwater wireless communication networks. *Phys. Commun.*, 1(3):163–182, September 2008.

[13] William H. Thorp. Analytic description of the low-frequency attenuation coefficient. *The Journal of the Acoustical Society of America*, 42(1):270–270, 1967.

[14] Ian F. Akyildiz, Dario Pompili, and Tommaso Melodia. Underwater acoustic sensor networks: Research challenges. *AD HOC NETWORKS (ELSEVIER*, 3:257–279, 2005.

[15] M. Speth, S. Fechtel, G. Fock, and H. Meyr. Optimum receiver design for OFDM-based broadband transmission .II. A case study. *Communications, IEEE Transactions on*, 49(4):571–578, April 2001.

[16] Milica Stojanovic, John G. Proakis, and Josko Catipovic. Analysis of the impact of channel estimation errors on the performance of a decision-feedback equalizer in fading multipath channels. *IEEE Transactions on Communications*, 43(234):877–886, 1995.

[17] Simon Haykin. *Communication Systems*. Wiley Publishing, 5th edition, 2009.

[18] Alejandro Cano-Gutierrez, Milica Stojanovic, and Josep Vidal. Effect of channel estimation error on the performance of svd-based mimo communication systems. In *Proceedings of the IEEE 15th International Symposium on Personal, Indoor and Mobile Radio Communications, PIMRC 2004, 5-8 September 2004, Barcelona, Spain*, pages 508–512. IEEE, 2004.

[19] Ian F.Akyildiz, 2012. Available at http://www.ece.gatech.edu/research/labs/bwn/UWASN/ Lastchecked:10 Oct, 2012.

[20] FAO. Study of acoustics, 2012. Available at http://www.fao.org/docrep/X5818E/x5818e04.htm Lastchecked:10 Oct, 2012.

[21] Stojanovic. Low complexity ofdm detector for underwater acoustic channels. In *OCEANS 2006*. M. Massachusetts Inst. of Technol., Cambridge, MA, 18-21 Sept 2006.

[22] Yik-Chung Wu * Rui Min. Joint channel estimation and data detection for multihop ofdm relaying system under unknown channel orders and doppler frequencies. *IEEE Communications Magazine*, (January):97–102, 2012.

[23] Bernhard Haeupler. Analyzing network coding gossip made easy. In *STOC*, pages 293–302, 2011.

[24] A.B. Carlson and P.B. Crilly. *Communication Systems*. McGraw-Hill, 2009.

[25] Artur Andrade Moura. Digital communications systems. Presentation Slides, MAP-Tele, FEUP, 2012.

[26] Manwinder Singh, Maninder Singh, and Anudeep Goraya. Article: Block based channel estimation algorithms for ofdm-ieee 802.16e (mobile wimax) system. *International Journal of Computer Applications*, 13(3):33–36, January 2011. Published by Foundation of Computer Science.